THE ASTROPHYSICAL JOURNAL, 256:460–480, 1982 May 15

ROTATION OF THE BULGE COMPONENTS OF DISK GALAXIES

JOHN KORMENDY
Dominion Astrophysical Observatory, Herzberg Institute of Astrophysics; and Kitt Peak National Observatory[1]
AND
GARTH ILLINGWORTH
Kitt Peak National Observatory[1]
Received 1981 June 3; accepted 1981 November 30

ABSTRACT

Absorption-line velocities and velocity dispersions have been measured along several slit positions in the bulge components of the edge-on S0–Sb galaxies NGC 4565, 4594, 5866, and 7814. These velocity fields, together with available data on four other objects, confirm indications from photometric studies that there exist significant dynamical differences between bulges and elliptical galaxies. The present bulges ($-18.5 \geq M_B \geq -21$) rotate more rapidly than bright ellipticals ($-19.5 \geq M_B \geq -23.5$; $H_0 = 50$ km s^{-1} Mpc^{-1}). Their kinematic properties are strikingly uniform and, in many cases, are well described by dynamical models of rotationally flattened oblate spheroids with isotropic residual velocities. Given that the disk potential also contributes to the flattening, little or no anisotropy is required to explain the shapes of bulges. Bulges are therefore unlike bright ellipticals, whose flattening is due to velocity anisotropies. However, a definitive comparison of bulges and ellipticals requires a kinematic study of ellipticals that are as faint as the present bulges. It is already clear that bulges and ellipticals have overlapping distributions of rotation properties. There is no dichotomy in the dynamics of elliptical and disk galaxies. The observation that bulges rotate rapidly suggests that they were formed by a dissipational process. In general, the detailed behavior of the two-dimensional velocity fields is consistent with classical dissipational collapse theories of galaxy formation.

The box-shaped bulge of NGC 4565 shows almost no decrease in rotation velocity up to large distances above the disk. In the remaining bulges the rotation rate decreases smoothly with increasing height above the plane. Thus, the box-shaped isophotes which are seen in some bulges may be associated with rapid, cylindrical rotation.

Subject headings: galaxies: formation — galaxies: internal motions — galaxies: structure

I. INTRODUCTION

The traditional picture of bulge components in spiral and S0 galaxies is that they are elliptical galaxies living in the middle of a disk. This view is based on the similarity of many basic properties of bulges and ellipticals, including morphology (Sandage 1961; Sandage, Freeman, and Stokes 1970), stellar content (Faber 1977), and the shape of the brightness profile (de Vaucouleurs 1959). Both components also have the same relationship $L \propto \sigma_0^n$, $n \sim 4$, between luminosity L and central velocity dispersion σ_0 (Faber and Jackson 1976; Sargent *et al.* 1977, hereafter S^{2}BS; Whitmore, Kirshner, and Schechter 1979; Whitmore and Kirshner 1981; Kormendy and Illingworth 1982). However, significant differences have now been found between the photometric structures of bulges and elliptical galaxies (Kormendy 1980; Boroson and Kormendy 1982, and references therein). To interpret these differences and to establish the nature of any dynamical distinction between bulges and ellipticals requires a study of their kinematics. In this paper we present stellar velocity fields and dispersion profiles of galaxy bulges and compare the dynamics of bulges and ellipticals.

Detailed kinematic data can be used to refine our picture of galaxy formation. This requires that we define the dynamical relationships between the major structural components of galaxies, i.e., the relation of ellipticals to bulges to disks. Disks are supported almost entirely by rotation. Their flattening is determined by the balance between rotation and the perpendicular velocity dispersion. It seemed natural in early models of ellipticals (Prendergast and Tomer 1970; Wilson 1975) to assume that they also had shapes determined by

[1]Operated by the Association of Universities for Research in Astronomy, Inc., under contract with the National Science Foundation.

rotation. However, recent work has shown that ellipticals rotate much less rapidly[2] than such models would predict (Bertola and Capaccioli 1975; Illingworth 1977; Peterson 1978*b*; Young *et al.* 1978; Schechter and Gunn 1979, hereafter SG; Davies 1981; Fried and Illingworth 1982). Almost simultaneously, Binney (1976, 1978) realized that initial asymmetries were probably preserved in the collapse of a protogalaxy. These results implied that anisotropy in the velocity distribution, and not rotation, determines the shapes of ellipticals. Thus, we see a striking dichotomy in the properties of ellipticals and disks. In ellipticals the initial random motion has been preserved, while in disks the dissipation during galaxy formation was strong enough to convert nearly all of the kinetic energy into ordered motion. It is therefore natural to ask whether bulges are objects with intermediate properties.

Preliminary data already suggest that bulges rotate faster than ellipticals. The central region of M31 has long been known to rotate rapidly (Babcock 1939; Rubin, Ford, and Kumar 1973; Pellet 1976; Peterson 1978*a*; Richstone and Schectman 1980). Also, Bertola and Capaccioli (1977) found that the bulge of the edge-on S0 NGC 128 rotates at ~ 150 km s^{-1} even 8″ up from the disk (8″ $= 3h^{-1}$ kpc, where $h = H_0/50$ km s^{-1} Mpc^{-1}, H_0 being the Hubble constant). This is comparable to the disk rotation rate. NGC 128 is an extreme example of a galaxy with a box-shaped bulge (Sandage 1961); one might expect rapid rotation in such objects (Freeman 1975). Finally, a particularly striking example is NGC 3115, whose bulge rotates almost as rapidly as predicted by oblate spheroid models in which the flattening is due to rotation (Illingworth and Schechter 1982). These results suggest that bulges may not be as similar to ellipticals as we have supposed. Therefore, we ask: to what extent do bulges rotate faster than ellipticals and more like the oblate models? In fact, are all of the photometric differences between bulges and ellipticals caused by the combined effect of rotation and the disk potential (see Kormendy 1980; Monet, Richstone, and Schechter 1981; Boroson and Kormendy 1982).

To address the above questions, we need bulge rotation curves that are uncontaminated by disk light. These can be measured in two ways. Either one can study bulges which are bright enough so that the disk contribution to the bulge rotation parameters is negligible (e.g., M31, M81), or one can study bulges in edge-on galaxies where the disk contribution can be clearly defined.

In this paper we study edge-on systems. Several slit positions have been used for each galaxy. First, the spectrograph slit was oriented parallel to the major axis but offset from the center to eliminate disk light. Spectra were also taken along the minor axis to define the radial gradient in velocity dispersion. Additional spectra parallel to the minor axis, but offset along the major axis, provide a measure of the drop in rotation velocity with increasing distance above the disk. We shall refer to these as perpendicular cuts. In general, sufficient spectra were taken to provide fairly detailed two-dimensional velocity fields.

[2]All statements concerning the importance of rotation (e.g., when we say, "... bulges rotate faster than ellipticals...") will refer to rotation in a dimensionless sense, where the normalizing factor is the velocity dispersion σ of the stellar component.

II. THE GALAXY SAMPLE

The galaxies studied are illustrated in Figure 1 (Plate 17) and included in Table 1. They were chosen to be larger than NGC 128 to eliminate disk contamination caused by poor seeing or guiding. They cover a range of Hubble types and bulge-to-disk ratios, but all have bulges that are large enough and round enough to dominate the light distribution far from the plane. However, of the 42 S0$^-$/ to Sbc/ galaxies listed in the RC2 (de Vaucouleurs, de Vaucouleurs, and Corwin 1976) which have total magnitudes $B_T \leq 12.5$ and declinations $\delta > -30°$, only four have bulges that are clearly thick enough for our purposes. We have measured all of these objects: NGC 4565, 4594, 5866, and 7814. Clearly, we are studying the least flattened objects in the tail of the distribution of bulge shapes. Yet it is of interest to note that these four bulges are at least as flattened as typical ellipticals. Recall that the distribution of true ellipticities of elliptical galaxies peaks near E4 (Sandage, Freeman, and Stokes 1970). The ellipticities of the edge-on bulges in Table 4 range from E3.7 to E5.7. Since these bulges are rounder than average, it appears that bulges may generally be flatter than elliptical galaxies when measured at surface brightnesses $\gtrsim 24B$ mag arcsec^{-2}. This result is in agreement with the conclusions of de Vaucouleurs (1974), Kormendy (1980), and Boroson and Kormendy (1982).

Basic properties of the galaxies studied are summarized in Table 1. Column (1) identifies the galaxy. Column (2) gives its morphological type from the RC2; edge-on galaxies are denoted "/". B/T in column (3) is the ratio of bulge to total luminosity, as quoted by sources given in column (4). Ratios followed by a colon are our own estimates based on the data of column (4); these should still be sufficiently accurate for our purposes. We note that B/T values are not corrected for internal absorption. Thus, for example, if NGC 4565 were seen face-on, the bulge would contribute a much smaller fraction of the light. Distances (col. [5]) are based on individual or (where available) group velocities and a Hubble constant of 50 km s^{-1} Mpc^{-1}. Velocities are taken from the RC2, and group memberships and group velocities from de Vaucouleurs (1975). Columns (6) and (7) give the total and bulge absolute magnitudes,

TABLE 1

BASIC PROPERTIES OF GALAXIES STUDIED

Galaxy (1)	Type (2)	B/T (3)	Source of Photometry[a] (4)	Distance (Mpc) (5)	$M_B(T)$ (6)	$M_B(B)$ (7)
NGC 224 (M31)	Sb	0.24	de Vaucouleurs 1958	0.65[b]	−20.12	−18.57
NGC 1553	S0	0.2:	(Freeman 1975)	20.0	−21.04	−19.3
NGC 3031 (M81)	Sab	0.28:	(Whitmore+1979)	3.3[c]	−20.09	−18.7
NGC 3115	S0$^-$/	0.84	Tsikoudi 1977	9.5	−19.93	−19.74
NGC 4565	Sb?/	0.35:	van Houten 1961; Hamabe+1980	18.9	−21.11	−19.97
NGC 4594 (M104) ...	Sa/	0.92	van Houten 1961	19.3	−22.26[d]	−22.17[d]
NGC 5866	S0$^+$/	0.9:	Hamabe+1979*a*, *b*	18.4	−20.47	−20.4
NGC 7814	Sab:/	0.9:	(van Houten 1961)	25.0	−20.73	−20.6

[a]Second and subsequent authors are abbreviated as +. References in parentheses indicate that we have derived B/T from data given in the reference, since the value of B/T was not explicitly quoted.

[b]From de Vaucouleurs 1978.

[c]From Tammann and Sandage 1968; Sandage and Tammann 1976.

[d]For consistency, $B_T = 9.27$ is taken from RC2. However, Burkhead's 1979 detailed photometry gives $B_T = 8.8$, implying $M_B(T) = -22.86$ and $M_B(B) = -22.77$.

TABLE 2

PARAMETERS OF SPECTRA

Parameter	2.1 m	4 m
Slit length (~110 pixels)	5′	2.′7
Scale along slit	~2.″7 pixel^{-1}	~1.″5 pixel^{-1}
Wavelength range (over 512 pixels) ...	~3880–4410 Å	
Dispersion	1 Å pixel^{-1} ≡ 75 km s^{-1} pixel^{-1}	
Resolution	~3.2 pixel FWHM[a]	
Instrumental velocity dispersion	$\sigma \approx 100$ km s^{-1}	
Limiting surface brightness in ~2 hr integration[b]	~24 *B* mag arcsec^{-2}	

[a]Full width at half-maximum.

[b]For an average of 10–20 rows, i.e., 15″–30″ at the 4 m telescope.

from B/T and from B_T values in the RC2, corrected for absorption as discussed by Burstein and Heiles (1978).

III. MEASUREMENT AND REDUCTION

a) Observations

All measurements were made with the High-Gain Video Spectrometer (HGVS) and the KPNO 2.1 m and 4 m telescopes. The observations required seven clear nights at the 2.1 m and 3.3 nights at the 4 m. Parameters of the spectra are given in Table 2.

The HGVS consists of the gold spectrograph and a silicon intensified target (SIT) detector (Ford 1979). Other than the camera head (SIT vs. ISIT) and the data format (128 rows of 512 pixels instead of 256 pixels square), the system is identical to the video camera (see the *KPNO Facilities Manual* and the HGVS manual). A three-stage RCA 73301 image tube provides intensification for the SIT camera. This large amount of intensification means that the data are, in principle, event-noise limited and not system-noise limited. However, in contrast to a photon-counting system, the system detective quantum efficiency does not closely approach the quantum efficiency of the first photocathode of the intensifier chain. The DQE is lowered because of problems such as the high weight of ion events, the width of the pulse height distribution, and the difficulty of fully removing the phosphor-imposed structure by flat-field division. Nevertheless, the system has a DQE considerably greater than that of conventional image tubes plus photographic plates.[3] This accounts for our faint limit-

[3]If a photographic image-tube spectrograph has sufficient gain to detect individual photons, then each photon is recorded as a clump of silver grains, greatly reducing the dynamic range. As a result, the gain is usually set low enough so that individual photons are not detected.

ing magnitude of ~ 1.5 mag arcsec^{-2} below sky in a 2–3 hr integration (Table 2).

Every 1.6 s the SIT is read and accumulated in a digital memory. While the photon gain of the system is much higher than that of integrating SIT systems (e.g., Westphal 1972; Ford 1979; SG), this very short integration time results in relatively smaller charge levels on the SIT target. This reduces to manageable levels the well-known velocity errors produced by the attraction of the electron readout beam by the charge distribution ("beam pulling"—see § III). The highest intensities that do not result in beam pulling correspond to $\sim 10\%$ of saturation. However, absorption-line velocities can be corrected for beam pulling at intensities up to $\sim 30\%$ of saturation, with accuracies of ~ 15 km s^{-1}. During an exposure, the accumulation memory also feeds a display memory and TV monitor, so the observer can see the image building up in real time. Finally, at the end of an integration, the spectrum is written onto disk memory and magnetic tape. To eliminate instabilities such as mechanical and magnetic flexure, a long exposure is accumulated as a series of 1024, 1.6 s integrations, i.e., in 27 minute segments, interspersed by short comparison arc exposures. During such exposures, the computer and display unit are free to do preliminary reduction and sky subtraction. Thus, observers can evaluate their data in real time with some confidence.

b) *Reduction*

Data reduction begins by removing the effects of the detector. Integrations containing only dark current and a DC offset are first subtracted from the data frames. To remove pixel-to-pixel variations in sensitivity, each frame is divided by the spectrum of a quartz incandescent lamp from which large scale variations have been removed. Along the slit, large scale variations in response are mapped and removed from the data by using separate spectra of blank sky. Object (but not comparison) spectra are cleaned of ion events. Full-slit HeNeAr comparison spectra are taken before and after each galaxy exposure; these are averaged and used to calculate the dispersion solution and to map the curvature. Generally, 15–17 lines are used; typical lines have an rms scatter of 4–8 km s^{-1} about the dispersion solution with no dependence on intensity. Individual lines generally deviate from the curvature solution by $\lesssim 10$ km s^{-1}. These errors are reduced in the overall solution because the deviations of different lines tend to cancel. In preparation for the final Fourier analysis the object data are rewritten using a spline interpolation procedure onto a $\ln \lambda$ scale, i.e., equal intervals in velocity. Tests show that it is safe to average individual 27 minute integrations, even when these were taken on different nights of the same run. The instrumental profile is clearly stable to a small fraction of a pixel, equivalent to velocity dispersions much smaller than our measurement limit of ~ 100 km s^{-1}. The last step in removing the detector from the data is to map and remove the S distortion, using the galaxy core or a nearby star. This correction is always small (≤ 3 pixels, often ≤ 1 pixel) and very well determined.

The most critical part of the reduction is sky subtraction. Most spectra reach the sky on both sides of the galaxy; the appropriate rows are then averaged to construct the sky spectrum. However, NGC 4594 and the major axes of several of the other galaxies fill the slit. Several sky spectra centered 1°–2° away from these objects were therefore interspersed with the galaxy exposures. Great care was taken to ensure that residual sky features were eliminated from the galaxy spectra as well as possible. Spectra with deliberately imperfect sky subtraction were reduced to verify that the above procedure is adequate. However, the sky subtraction is usually poor for the strongest emission lines. The Fourier velocity program therefore interpolates linearly through 20 Å regions centered on the lines Hg $\lambda\lambda$4046 and 4358 and occasionally the twilight line at λ3915.

The procedure described above was also used to observe and reduce the spectra of G8-K2 III stars used as velocity standards. To eliminate beam pulling, the stars were reduced in brightness by using neutral density filters and by rapid trailing along the slit. Star spectra were reduced in the same way as galaxy spectra and then averaged into a high signal-to-noise (S/N) 1×512 pixel format. These spectra and the 128×512 pixel, sky-subtracted galaxy spectra are the input data for the Fourier velocity program.

Some 150 two-dimensional spectra were reduced as above by a mixture of batch and interactive procedures, the latter requiring nearly 250 hr of terminal time. Programs involving two-dimensional data reduction should not be undertaken lightly.

c) *Analysis*

The next step in the data reduction consists of calculating velocities and dispersions. This is done with a Fourier quotient program originally written and kindly made available by P. Schechter. The Fourier quotient technique is described in detail in S^{2}BS and in SG. In essence, the galaxy spectrum is assumed to equal the convolution of the standard star spectrum with a Gaussian broadening function shifted in wavelength by the velocity difference between galaxy and star. The ratio of the Fourier transforms of the galaxy and star spectra therefore gives the Fourier transform of the broadening function. A three-parameter Gaussian fit is then made to this quotient, yielding for each radius interval the radial velocity V relative to the star, the velocity dispersion σ, and the overall ratio γ of the line strengths in the galaxy and the star. We also have error estimates for all of these quantities based on the quality of the Gaussian fit to the Fourier quotient. Next, the raw profiles of V,

σ, and γ are folded about the photometric symmetry point to produce the results discussed in the next section. This process also removes the systemic velocity. When data on a particular slit position were obtained over several runs, the last step in the reduction is to average all the folded data.

The Fourier quotient program has been thoroughly tested by Sargent *et al.* (1977), Schechter and Gunn (1979), and Fried and Illingworth (1982). We could see no advantage in using the cross-correlation technique discussed by Tonry and Davis (1979). Recently, Efstathiou, Ellis, and Carter (1980) have shown that in practice neither the S^2BS Fourier-quotient method nor the Tonry-Davis CCF method possesses a real advantage in the accuracy to which one can determine velocities and velocity dispersions. Only at the highest and lowest velocity dispersions tested could one see a slight preference for one technique over the other. In fact, at the low dispersions relevant in this paper, the Fourier quotient technique appeared to give more consistent results, i.e., the dispersions were less dependent on model parameters than values derived with the CCF method. The results show that the Fourier-quotient technique gives high-quality velocities and dispersions, with little systematic dependence on the standard star used or on the S/N of the object data. In addition, we have performed a number of tests. These, and the procedures used to overcome some problems with the data, are described below.

Ca II *H and K lines.*—The wavelength region chosen for this study (3880–4410 Å) includes the very strong H and K lines of Ca II. Tests during analysis showed that inclusion of these features resulted in slightly inconsistent, overestimated dispersion measurements, in accordance with the experience of Schechter (1981) and of Fried and Illingworth (1982). We have removed from the analysis a region of width ~ 60–80 Å around H and K. This typically lowers σ by $\sim 20\%$ and produces values which are consistent with data from different observing sessions and other authors. H and K are strong, intrinsically broad features that lie in a region of very steep spectral flux gradient. It seems not unlikely that a slight mismatch between the galaxy and comparison star in either the intrinsic strength of H and K or in the steep continuum gradient in this region could effect the measured dispersion. (The value of the Fourier-quotient technique has, in general, been that one is *not* dependent upon critical matching between a small number of features.) Similarly, Fried and Illingworth (1982) obtained good agreement in velocity dispersion measurements between spectra in markedly different spectral regions only by removing H and K from the derivation. Taken together, the above arguments justify the elimination of these lines. On the other hand, the inclusion or omission of H and K has no effect on the velocity, except that higher S/N and more accurate velocities are obtained when H and K are included. We have therefore reduced all of the data twice, once with H and K to derive velocities and once without these lines to measure dispersions.

Standard star.—Our standard star sample included G8 III, K0 III, K1 III, and K2 III stars. G8 III stars gave dispersions that were systematically low by 12% compared with results from later type stars. This is the same order of uncertainty seen by previous authors (SG; S^2BS) as the spectral type is varied away from the best match. It indicates the need for some care in the choice of stellar comparison objects. The K0–K2 III spectra appeared to give the best match to the galaxy data and were subsequently used as standards. Results calculated with different K0–K2 III stars differ by $\pm 3\%$ (rms) in $\Delta V/V$ and in $\Delta\sigma/\sigma$. In contrast to work on nuclear dispersions (S^2BS), it is impractical to reduce all of the data with many different stars and then to average the results. However, we have reduced a large fraction of the data with two or three different stars to verify that the dependence on standard star is acceptably small. The adopted results are generally calculated by using the highest S/N star measured on the same night as the galaxy.

Beam pulling.—The position of the read beam on the target of a vidicon depends on the local charge density. As noted above, we find that illumination levels exceeding $\sim 10\%$ of saturation produce measurable beam pulling. This error is roughly proportional to the local intensity, with a smaller additional dependence on the form of the brightness distribution. In the present observations beam pulling is significant only within $\sim 15''$ of the center of the major axis of NGC 4594. The error can readily be determined and removed by assuming that velocity fields are generally symmetric about the nucleus. An observed asymmetry of the rotation curve is then produced because beam pulling has the same sign on both sides of the center. Symmetrizing all high-intensity rotation curves (including M32; see § IV) yields a correction curve for each spectrum. The average of these has been used to correct the central four points ($0'' \leq r \leq 14''$) of the major-axis rotation curve of NGC 4594. The maximum correction was 60–70 km s^{-1} for the $r = 0''$ point. We emphasize that these were the only data in this paper that required a correction. Beam pulling therefore has no effect on any of our conclusions. As expected, its effect on the velocity dispersion is even smaller; in fact, it is undetectable.

Scattered light.—Like all image-tube systems, the HGVS suffers from internal scattered light. This manifests itself as a featureless, uniform background at a level of $\sim 1\%$ of that in the incident spectrum. Scattered light is a problem only for spectra with very steep brightness gradients, i.e., those centered on the nuclei of galaxies. Consistency checks (see § IV) and experiments have shown that velocity and dispersion measurements

are unaffected by this uniform background. However, the line strength parameter γ sometimes displays radial gradients which result from dilution by scattered light. Spectra that suffer from this effect are flagged (*) in Table 3. Variations in γ should therefore not be interpreted as real gradients in line strength. Work to remove this problem is planned as a part of a study of line strengths in bulges.

Our tests, the direct comparison of internal and external errors by Schechter (1980), and the comparison of the Fourier-quotient method with the cross-correlation method made by Efstathiou, Ellis, and Carter (1980) leave us confident that the error estimates given in the next section are realistic.

IV. KINEMATIC DATA ON EDGE-ON GALAXIES

Final rotation velocities V, dispersions σ, and line strengths γ in NGC 4565, 4594, 5866, and 7814 are listed in Table 3 and illustrated in Figure 2. Also given are the errors in these quantities, $\epsilon(V)$, $\epsilon(\sigma)$, and $\epsilon(\gamma)$. Negative radii in Table 3 refer to points whose position angles with respect to the nucleus are $0° \leq \theta < 180°$ (north through east). Each set of measurements is identified by the displacement of the slit from the nucleus in arcseconds and by the orientation of the slit, either parallel ($\|$) or perpendicular ($\perp$) to the major axis. The total integration time at each slit position is given after the identification, followed by the number of 1024-read integrations in parentheses.

The rotation curves, dispersion profiles, and "line strength" variations are plotted in Figure 2. In all cases the dispersion and line strength data, but not the rotation data, are derived with H and K removed from the spectra. As a result, there are sometimes differences in the number of V and σ data values.

All of the data are folded about a photometric symmetry point, i.e., the center of the galaxy, the minor axis, or the disk. In addition, the rotation velocity data for the major axis, the parallel cuts, and the minor axis have been reflected through the zero velocity point. The minor axis spectra are folded in this way so as to search for any systematic rotation; such rotation is predicted by some models of triaxial ellipsoids. The velocity zero point is established by comparing the velocities on either side of the point about which the data were folded. No significant asymmetry in the velocity data can be seen. The perpendicular cuts are treated a little differently. In these the velocities on both sides of the disk decrease (or increase) toward the systemic velocity as the radii increase. These data are folded about the $z = 0''$ point, as defined by the photometry. Their velocity zero points are set by requiring good agreement with the velocities in the intersecting parallel cuts.

Wherever two slit positions cross, we have two independent measurements of the velocity dispersion. On each panel in Figure 2 the dispersions derived from all intersecting slit positions have been plotted as crosses. Those crosses without error bars are measured on a smooth curve drawn through the dispersion profile along the intersecting slit position. However, along the minor axis, each cross is actually the $r = 0''$ dispersion point from the intersecting parallel cut, complete with error bar. Examining the figures shows that the dispersions are extremely consistent. The only exception is the data along the 40″ parallel cut in NGC 4594, which gives dispersions that are systematically too large by 41 ± 13 km s^{-1}. However, these data represent only 27 minutes of integration and are therefore not very accurate. All other crosses agree with the intersecting cuts to within the errors. We emphasize that this is true despite the fact that the intersecting slit positions were often measured with different telescopes, different SIT detectors, and especially, on different observing runs as much as nine months apart. Thus, the internal consistency of the dispersion data is excellent, comparable to or better than the error bars shown. This internal consistency also supports the claim in § III that scattered light has not systematically affected the velocity dispersion data.

External consistency checks are possible for two of our dispersion measurements. In the central 1″.5 of NGC 4594 we obtain $\sigma = 256 \pm 22$ km s^{-1}. (This is not evident in Table 3 because the dispersion gradient is large and because several points near the center have been averaged.) For comparison, Whitmore, Kirshner, and Schechter (1979) obtained $\sigma = 263 \pm 32$ km s^{-1}, also using a Fourier quotient program. On the other hand, Williams (1977) derived $\sigma = 215 \pm 35$ km s^{-1} using a visual technique and a composite standard spectrum. However, Williams's (1977) dispersions are systematically lower than those derived more recently by a variety of techniques (S^2BS; Whitmore, Kirshner, and Schechter 1979; Terlevich *et al.* 1981). A more stringent test is provided by an object with a lower velocity dispersion. We have therefore measured the dispersion near the nucleus of M32 and obtained $\sigma = 88 \pm 6$ km s^{-1}. This value is consistent with other measurements; S^2BS derive $\sigma = 83 \pm 3$ km s^{-1} and 84 ± 6 km s^{-1} from two different spectral regions. However, the true dispersion is probably slightly smaller; more recent measurements at an instrumental σ of $\sigma \approx 60$ km s^{-1} give a central dispersion for M32 of $\sigma = 67 \pm 5$ km s^{-1} (Kormendy 1982*a*). This is symptomatic of the fact that Fourier quotient results become overestimates as the true dispersion falls significantly below the instrumental dispersion (see SG). This effect is important even at the high S/N of the M32 measurements. It is still more pronounced at low S/N, where $\sigma_{\text{measured}} \to \sigma_{\text{instrumental}}$ as $\sigma_{\text{true}} \to 0$. Thus, low S/N measurements giving $\sigma \lesssim 100$ km s^{-1} are essentially upper limits.

With this exception, our results are consistent with the velocity dispersion system defined by Fourier-quotient and power-spectrum techniques. Terlevich *et al.*

TABLE 3

ROTATION, DISPERSION, AND LINE STRENGTH DATA

r	V	ε(V)	σ	ε(σ)	γ	ε(γ)
NGC 4565 12" ‖ 82 min (3)						
-155.2	-270	39	...	...	...	...
-135.9	-218	34	...	...	...	...
-106.4	-166	17	...	...	...	...
-81.3	-164	15	92	27	0.40	0.05
-55.7	-138	14	73	24	0.38	0.04
-37.3	-114	14	91	26	0.43	0.05
-24.8	-87	12	112	19	0.53	0.05
-12.3	-41	11	150	14	0.66	0.05
0.0	1	9	157	12	0.71	0.05
12.2	41	10	145	14	0.66	0.05
24.8	82	11	114	15	0.65	0.05
37.3	107	11	89	18	0.52	0.04
55.4	141	13	74	26	0.38	0.04
81.0	147	28	62	54	0.24	0.05
108.9	200	20	129	34	0.33	0.05
138.6	238	26	134	47	0.30	0.07
NGC 4565 34" ‖ 191 min (7)						
-96.2	-80	44	...	...	...	...
-46.1	-83	20	93	33	0.51	0.07
-30.6	-68	18	98	35	0.52	0.08
-14.9	-53	20	184	28	0.80	0.11
-8.5	-15	14	66	30	0.82	0.07
8.3	18	11	62	27	0.51	0.05
25.8	64	18	57	44	0.44	0.07
49.5	122	20	65	56	0.45	0.08
NGC 4565 Minor Axis 82 min (3)*						
-38.8	10	16	141	21	0.70	0.07
-25.8	26	11	109	17	0.66	0.06
-4.3	-19	10	159	13	0.96	0.07
0.0	-3	10	150	10	1.05	0.07
4.5	-8	8	174	9	1.05	0.06
9.0	-8	10	169	12	0.96	0.06
14.2	3	8	145	11	0.88	0.05
21.5	9	8	102	14	0.76	0.05
35.6	20	16	86	27	0.54	0.07
NGC 4565 27" ⊥ 109 min (4)						
-50.2	-15	38	65	72	0.65	0.17
-40.0	51	16	111	26	0.71	0.08
-30.0	92	18	82	32	0.75	0.10
-16.1	88	26	171	38	0.54	0.09
-5.7	103	9	119	14	0.85	0.05
0.0	99	8	113	11	0.92	0.05
6.1	81	8	107	12	0.85	0.05
14.9	87	8	111	12	0.84	0.05
29.1	60	17	76	32	0.68	0.09
NGC 4594 Major Axis 82 min (3)*						
-120.7	338	42	...	...	...	...
-76.2	...	...	95	36	0.40	0.06
-67.9	274	11	...	...	...	...
-44.9	256	9	121	14	0.50	0.03
-33.5	218	11	135	15	0.60	0.04
-24.4	183	12	168	16	0.59	0.05
-14.0	132	9	...	...	...	...
-13.6	...	...	218	12	0.78	0.04
-7.2	117	10	216	11	0.89	0.05
-2.7	87	10	225	11	0.90	0.05
0.0	-3	16	...	...	...	...
1.8	...	...	208	10	0.72	0.04
2.7	-99	11	...	...	...	...
6.7	-127	11	185	13	0.66	0.04
13.0	-129	11	206	15	0.69	0.04
20.4	-165	12	146	15	0.53	0.04
33.6	-234	10	145	12	0.57	0.03
47.5	-240	10	101	16	0.50	0.03
70.5	-243	8	110	13	0.39	0.02
121.3	-233	36	127	52	0.27	0.06
NGC 4594 30" ‖ 82 min (3)						
-89.3	124	28	...	...	...	...
-59.9	83	15	235	20	0.54	0.05
-34.7	89	13	222	19	0.59	0.05
-15.4	25	12	236	16	0.57	0.04
0.0	-7	13	205	17	0.57	0.04
15.3	-43	12	215	17	0.57	0.04
34.2	-56	17	240	22	0.51	0.05
56.0	-69	17	203	23	0.47	0.05
78.5	-95	25	228	32	0.43	0.06
NGC 4594 40" ‖ 27 min (1)						
-62.1	94	30	230	37	0.60	0.09
-37.0	78	24	266	31	0.77	0.10
-17.4	-12	31	270	41	0.60	0.10
0.0	-43	24	272	29	0.81	0.09
17.3	-5	22	211	29	0.58	0.07
37.0	-42	28	273	32	0.85	0.11
64.7	-50	38	238	49	0.46	0.09
NGC 4594 50" ‖ 109 min (4)						
-44.5	27	16	210	21	0.59	0.06
-15.9	28	14	234	18	0.71	0.06
0.0	-12	23	195	27	0.59	0.07
17.8	-16	14	239	16	0.73	0.05
43.3	-17	14	205	18	0.62	0.05
76.1	-53	20	214	26	0.50	0.06
NGC 4594 Minor Axis 55 min (2)*						
-54.2	8	26	186	40	0.18	0.03
-25.5	0	12	251	16	0.55	0.04
-7.6	-11	8	182	11	0.67	0.04
10.5	10	10	174	14	0.52	0.04
38.6	1	22	209	31	0.38	0.05
67.0	20	22	176	29	0.22	0.03
NGC 4594 50" ⊥ 55 min (2)						
-50.2	38	23	189	29	0.34	0.04
-27.1	62	20	186	27	0.46	0.05
-16.6	103	19	177	23	0.53	0.05
-10.6	141	17	156	20	0.62	0.05
-6.1	223	14	176	17	0.81	0.06
-2.3	270	14	95	22	0.61	0.06
0.8	271	12	124	19	0.74	0.06
5.1	252	17	...	...	...	...
10.4	167	24	153	31	0.53	0.07
27.5	100	29	196	37	0.38	0.06
42.9	30	28	239	35	0.50	0.07
70.3	7	33	166	43	0.30	0.05
NGC 5866 14" ‖ 55 min (2)						
-55.8	92	23	118	31	0.35	0.05
-37.2	76	11	110	18	0.37	0.03
-22.1	47	10	138	14	0.57	0.04

TABLE 3—*Continued*

r	V	ε(V)	σ	ε(σ)	γ	ε(γ)
-11.6	2	9	152	14	0.67	0.04
-5.1	1	10	156	14	0.71	0.05
0.0	11	13	175	16	0.76	0.06
5.2	3	9	136	14	0.67	0.04
12.2	-17	8	132	13	0.65	0.04
22.4	-37	9	138	13	0.59	0.04
38.6	-84	11	176	14	0.64	0.04
54.6	-110	22	121	33	0.41	0.06
70.2	-143	20	114	34	0.33	0.04
NGC 5866	22" ‖		137 min (5)			
-58.8	87	13	126	21	0.70	0.06
-38.2	55	11	166	14	0.84	0.05
-22.4	35	9	148	13	0.87	0.05
-12.5	11	9	120	13	0.75	0.04
-5.7	-17	10	139	15	0.83	0.05
0.0	11	11	147	17	0.87	0.06
5.4	21	9	144	14	0.90	0.05
12.0	-11	9	139	13	0.90	0.05
23.8	-47	11	124	15	0.68	0.04
37.3	-56	9	162	13	0.86	0.05
55.5	-68	12	145	18	0.73	0.05
75.1	-115	29	154	40	0.53	0.08
NGC 5866	Minor Axis		55 min (2)			
-21.6	22	15	146	24	0.71	0.07
-14.4	11	9	127	14	0.85	0.05
-7.7	3	7	168	10	0.97	0.04
-3.9	-1	9	161	12	0.92	0.05
0.0	-14	8	170	11	0.96	0.05
3.8	-13	9	152	12	0.92	0.05
8.1	-6	7	151	9	0.91	0.04
14.3	15	9	154	13	0.95	0.05
21.7	11	16	116	26	0.62	0.06
NGC 5866	25" ⊥		55 min (2)			
-39.2	...	...	184	52	0.79	0.19
-26.2	23	23	155	33	0.65	0.10
-18.8	44	17	138	25	0.65	0.08
-13.6	85	11	120	19	0.74	0.06
-9.9	88	13	124	21	0.64	0.06
-6.8	103	15	159	21	0.71	0.07
-3.0	132	12	136	18	0.73	0.06
0.0	154	13	118	21	0.65	0.06
2.3	125	13	146	16	0.75	0.06
5.3	115	14	150	19	0.79	0.07
8.3	90	14	152	21	0.75	0.07
12.7	50	13	148	19	0.74	0.07
18.8	37	19	163	25	0.77	0.09
25.5	5	20	125	34	0.70	0.09
34.3	...	...	132	51	0.75	0.17
NGC 7814	4" ‖		109 min (4)			
-65.9	174	22	32	85	0.60	0.12
-40.4	102	21	168	30	0.81	0.11
-22.9	88	16	159	23	0.75	0.08
-6.8	54	9	152	13	0.81	0.05
0.0	-2	14	168	20	0.83	0.08
7.2	-50	9	173	13	0.85	0.05
24.5	-102	16	136	26	0.71	0.08
50.9	-100	20	90	32	0.73	0.10
NGC 7814	12" ‖		109 min (4)			
-70.0	138	45	124	66	0.40	0.12
-37.9	57	20	169	30	0.67	0.10
-13.4	46	13	154	20	0.60	0.06
0.0	-4	15	160	21	0.77	0.08
13.2	-38	11	124	18	0.61	0.05
49.2	-60	21	108	39	0.46	0.08
NGC 7814	18" ‖		218 min (8)			
-96.4	...	...	67	62	0.41	0.10
-90.8	119	29	...	...	...	...
-50.5	76	22	118	35	0.49	0.08
-27.0	55	13	106	22	0.64	0.06
-11.1	28	12	101	20	0.76	0.07
0.0	5	12	114	19	0.73	0.06
11.5	-34	12	106	19	0.84	0.07
24.6	-45	15	98	27	0.67	0.08
35.4	-70	21	124	32	0.64	0.10
51.8	-87	22	...	...	...	...
64.7	-67	31	91	51	0.44	0.11
NGC 7814	Minor Axis		55 min (2)			
-32.5	11	27	142	40	0.56	0.11
-19.5	-3	13	99	22	0.71	0.08
-8.7	-6	10	152	14	0.87	0.06
0.2	10	14	167	18	0.85	0.08
8.6	-13	13	151	17	0.80	0.07
19.5	13	21	134	33	0.60	0.10
31.5	100	35	129	58	0.53	0.15
NGC 7814	20" ⊥		82 min (3)			
-35.1	12	33	203	46	0.92	0.18
-20.8	68	16	112	24	0.69	0.08
-9.4	56	17	124	24	0.72	0.08
0.4	80	22	109	36	0.64	0.11
9.1	65	15	135	20	0.79	0.08
20.6	23	21	111	33	0.64	0.10
35.2	30	34	92	63	0.50	0.15
NGC 7814	40" ⊥		109 min (4)			
-30.5	20	36	126	47	0.79	0.18
-22.8	90	28	125	42	0.86	0.17
-17.4	90	31	111	51	0.61	0.14
-12.1	111	26	156	37	0.76	0.13
-8.1	146	21	69	38	0.72	0.12
-5.4	99	27	98	46	0.72	0.15
-2.7	104	36	73	68	0.52	0.15
2.7	102	34	131	48	1.04	0.23
5.4	105	24	140	37	1.05	0.18
8.1	69	25	127	37	0.95	0.16
12.1	90	20	102	31	0.82	0.12
17.4	48	29	152	44	0.75	0.15
22.8	32	30	125	47	0.81	0.18
30.5	45	32	160	44	1.09	0.21

NOTES: Radius r is in arcseconds with negative values being east of a N-S line.
V, ε(V), σ, and ε(σ) are in km s^{-1}.
Major-axis position angles: NGC 4565 - 135°; NGC 4594 - 90°; NGC 5866 - 126°; NGC 7814 - 134°.
* Indicates a scattered light problem with γ (§ III).

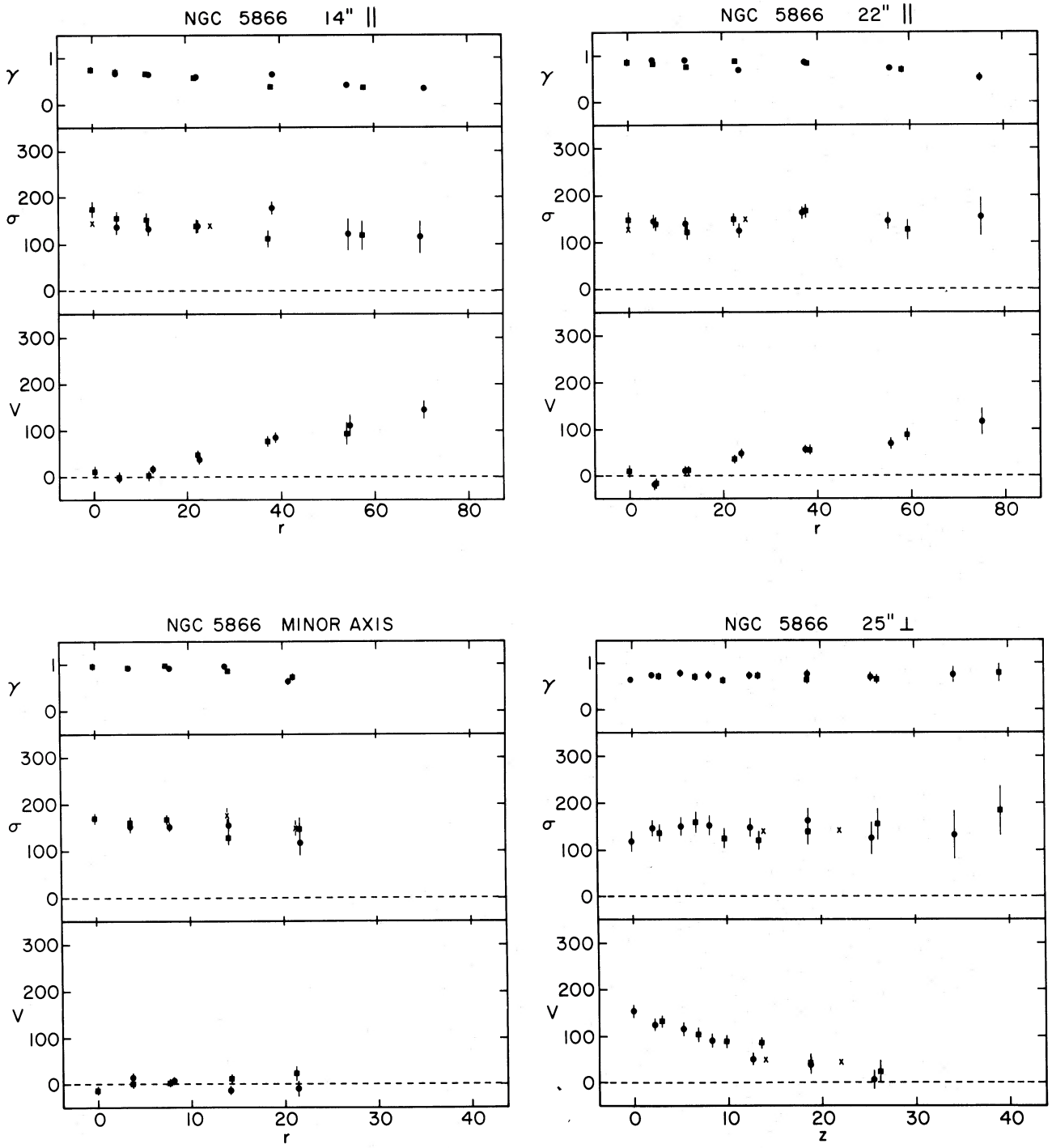

FIG. 2*a*.—Rotation velocities V, dispersions σ, and line strengths γ for NGC 5866. Slit positions for each data set are given in the title; ⊥ indicates slits perpendicular to the major axis, while || indicates slits parallel to the major axis. Appropriate offsets are given in seconds of arc; see Fig. 1. All velocities are in km s^{-1}. The dimensionless line strength factor γ is discussed in the text. All radii are in seconds of arc. Scale is $11h$ arcsec kpc^{-1} ($h = H_0/50$ km s^{-1} Mpc). All data are folded about the nucleus, with different sides being represented by filled circles and filled squares. Crosses are derived from intersecting slit positions and serve as consistency checks (see § IV).

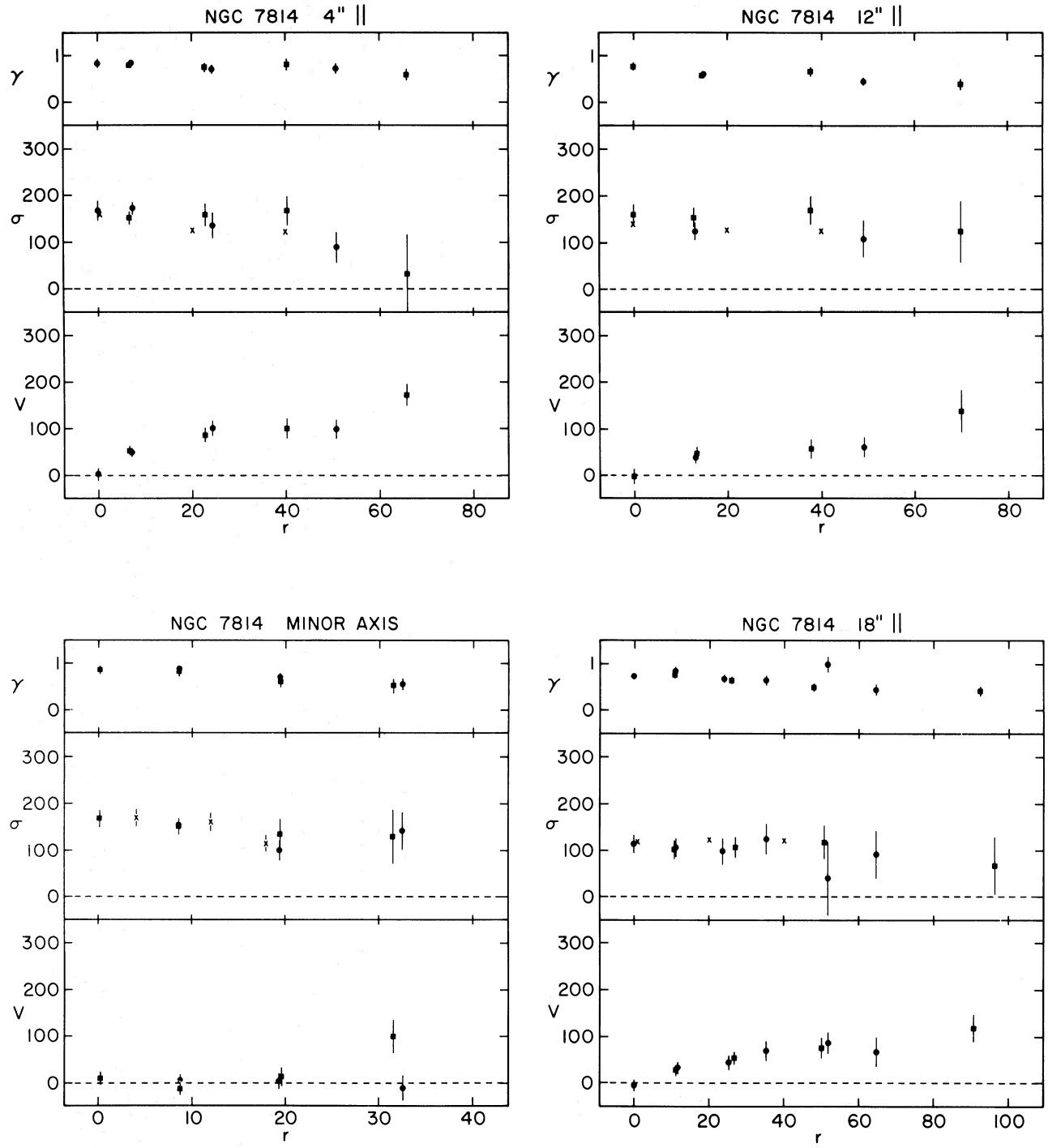

FIG. 2*b*.—Same as Fig. 2*a*, but for NGC 7814. Scale is 8.3*h* arcsec kpc^{-1}.

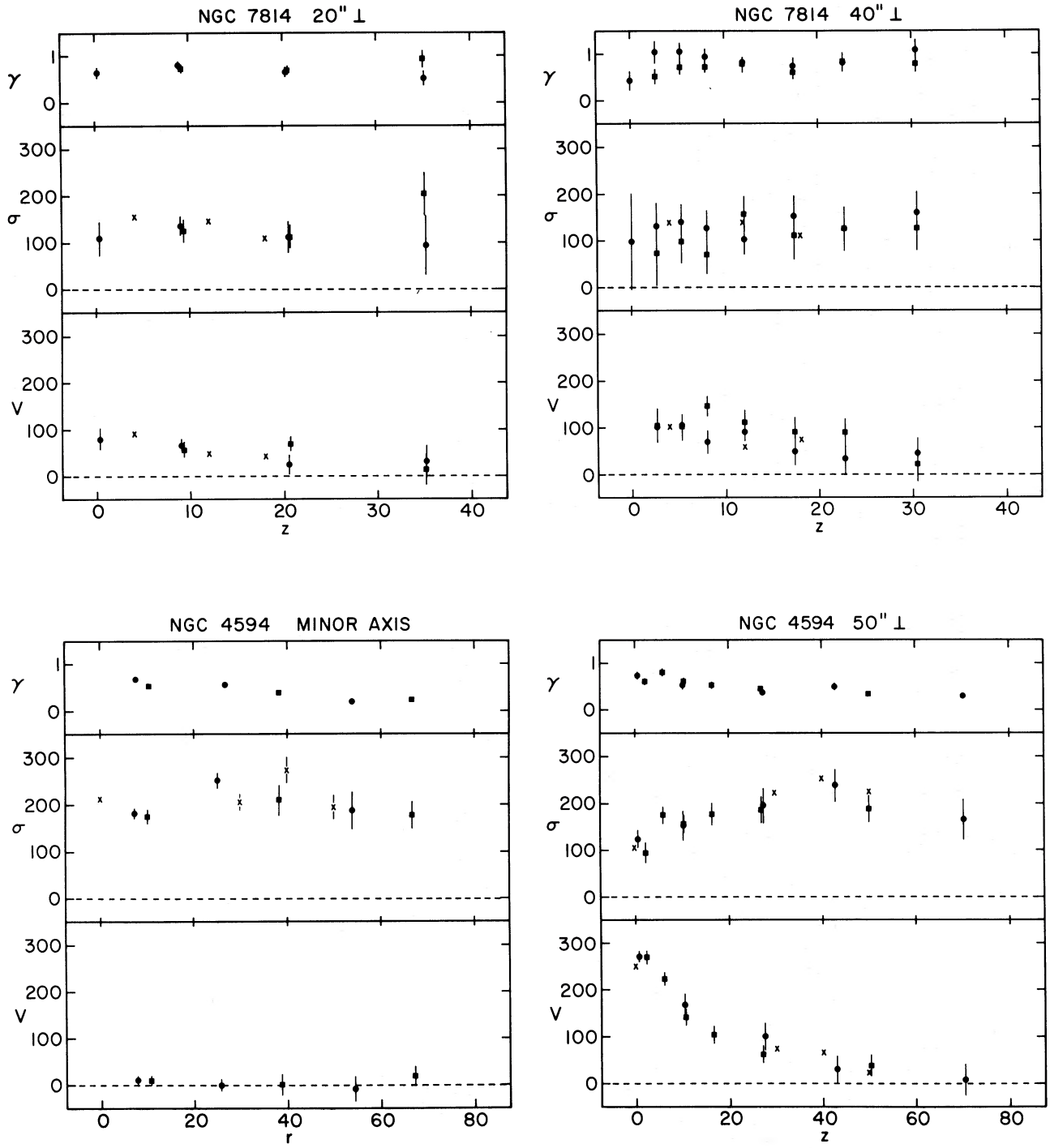

FIG. 2*c*.—Same as Fig. 2*a*, but for NGC 4594 and 7814. Scale for NGC 4594 is 11*h* arcsec kpc^{-1}.

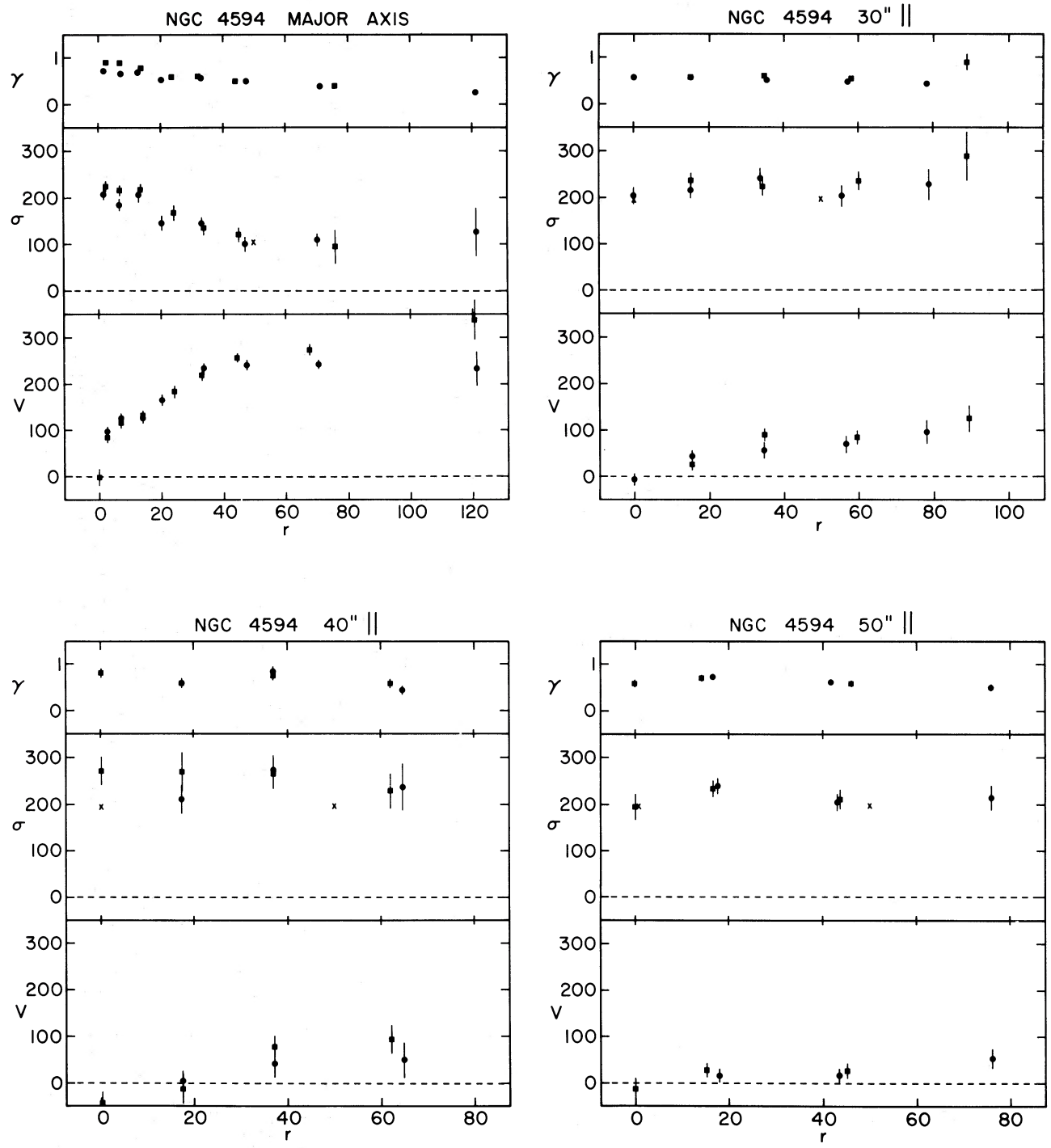

FIG. 2*d*.—Same as Fig. 2*a*, but for NGC 4594

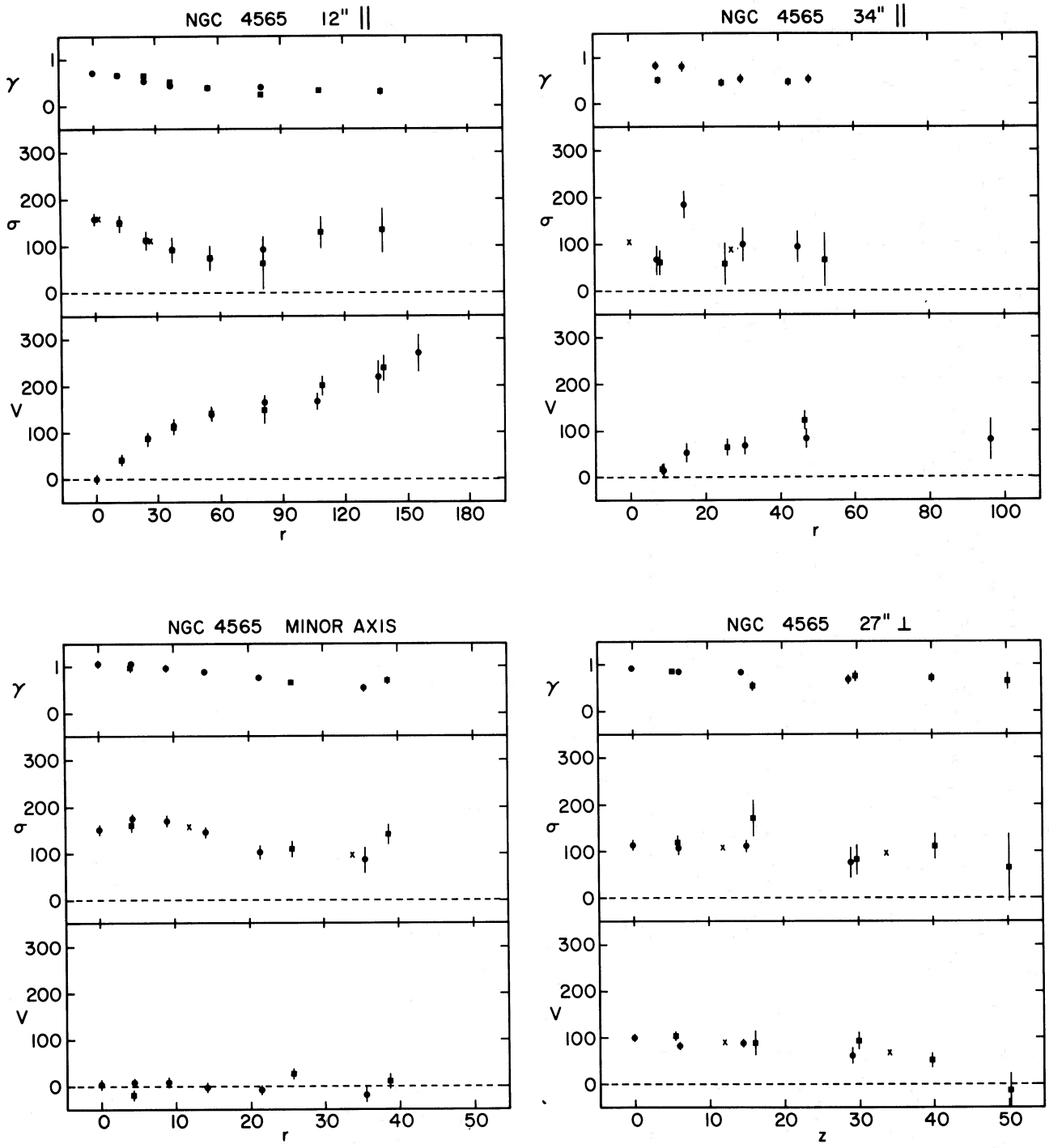

FIG. 2e.—Same as Fig. 2a, but for NGC 4565. Scale is 11h arcsec kpc^{-1}.

(1981) and Illingworth (1981) have shown that these techniques generally measure dispersions consistent to $<10\%$.

Turning next to the velocities, we note that measurements along the perpendicular and parallel cuts are not independent, because the latter set the zero point of the former. For this reason, velocities from the perpendicular cuts are not plotted on the parallel-cut rotation curves in Figure 2. However, the parallel cuts taken together independently define the z velocity gradient. We illustrate this consistency check by plotting interpolated velocities from the parallel cuts as crosses on the perpendicular-cut data. The agreement is again seen to be excellent. Thus, the internal consistency of the velocity data is good.

Very few external consistency checks can be made on our velocities. The only published absorption-line rotation curve which is directly comparable to our own is that of NGC 4594 (Faber *et al.* 1977). Their data and the measurements in Table 3 are in good agreement. However, the emission-line velocities measured by Schweizer (1978) are higher than both sets of absorption-line velocities by 50 km s^{-1} at all radii greater than $\sim 40''$. Schweizer's emission-line velocities at large radii agree with the H I velocity width measured by Faber *et al.* (1977). The most likely interpretation of this difference is that the observed low stellar velocities result from contamination of the disk light by the slower rotating, hot bulge.

V. RESULTS

This section will describe the qualitative kinematics of our galaxies in two parts, (*a*) a summary of the properties common to all of the galaxies, and (*b*) a more detailed discussion of individual features. Section VI gives an analysis of the dynamical implications. No effort is made to deproject the data; observations are compared with dynamical models that have been projected onto the sky.

a) *General Properties*

The common features of all the galaxies are those with the most far-reaching implications (see Fig. 2).

1. Fairly rapid rotation is seen in the bulges even at distances of several kpc above the disk. In fact, the rotation velocity approaches the global velocity dispersion in magnitude, $V/\langle\sigma\rangle \approx 0.6$–$0.9$.

2. The rotation velocity decreases very smoothly with increasing distance from the disk. There is no sharp distinction in rotation properties between the bulge and disk component.[4] Such a distinction is seen only in the photometry.

[4]Schweizer (1981) points out that a smooth transition between disk and bulge rotation rates is also a well-known property of the stellar populations in our Galaxy (e.g., Blaauw 1965; Oort 1965).

3. The rotation velocities measured parallel to the disk but displaced in z rise more slowly and more linearly with radius than the major-axis velocities.

4. No rotation is seen along the minor axis of any of these bulges.

5. The velocity dispersions but then change only slowly, if at all, throughout the bulge.

b) *Specific Features*

i) *NGC 5866*

The S0$^+$ galaxy NGC 5866 is prototypical of the above behavior (Fig. 2*a*). At $z = 22'' = 2\ h^{-1}$ kpc, the rotation curve rises to nearly 100 km s^{-1}. This is comparable to the mean dispersion $\langle\sigma\rangle \approx 150$ km s^{-1} in the bulge. The continuous gradient in rotation with z is well illustrated by the 25″ perpendicular cut. These data indicate that the maximum disk rotation rate is at least 160 km s^{-1}. The actual value is probably higher because the disk is obscured by dust, and because we are integrating line-of-sight velocities through the disk. However, no direct measurement of the circular velocity is available because NGC 5866 has not been detected in H I or in optical emission.

ii) *NGC 7814*

NGC 7814 is morphologically very similar to NGC 5866 (Fig. 1). Both galaxies have a prominent edge-on dust lane, but the disk is fainter in NGC 7814 than in NGC 5866. In this object we have three parallel and three perpendicular cuts, giving a fairly detailed velocity field. The kinematic behavior (Fig. 2*b*, *c*) is very similar to that of NGC 5866. Again there is considerable rotation even $18'' = 2\ h^{-1}$ kpc above the disk plane, with a smooth decrease in velocity with height. To avoid the dust lane, the major-axis slit position was offset by 4″ in z. The maximum velocity seen in this spectrum out to $50'' = 6\ h^{-1}$ kpc is ~ 100 km s^{-1} (we give low weight to the point at 170 km s^{-1}). This is considerably smaller than the maximum H I velocity in the disk, $V = 245$ km s^{-1} (Bottinelli, Gouguenheim, and Paturel 1980). Part of the reason may be that our data do not reach large enough radii and that they integrate the line-of-sight velocities through the disk. However, it is also likely that the disk is so thin and so heavily absorbed that it contributes little light to our 4″-offset major-axis spectrum.

iii) *NGC 4594*

As Figures 2*c*, *d* show, some rotation (50 km s^{-1}) is still seen even 50″ (5 h^{-1} kpc) above the disk plane. Again the rotation curve is more linear along the offset parallel cuts than along the major axis. Velocities decrease smoothly along the 50″ perpendicular cut; how-

ever, the data near $z = 0$ are dominated by the rotation of the disk, which is not quite edge-on. The effect of the disk is clear in the velocity dispersions, which do not rise to values $\sigma \approx 210$ km s^{-1} characteristic of the bulge until $z \approx 15''$. (The dispersions $\sigma \approx 100$ km s^{-1} seen in regions dominated by the disk are not representative of the true disk dispersion because of residual bulge contamination and line-of-sight integration effects.) The bulge velocity dispersion is remarkably constant at $\sigma = 210$ km s^{-1}, except in the central several arcseconds, where there is a rapid increase to 256 ± 22 km s^{-1} (§ IV).

iv) *NGC 4565*

Undoubtedly the most interesting bulge in our sample is that of NGC 4565. Its isophotes are distorted into a "box-shaped" structure (Fig. 1) similar to that seen in a number of other galaxies, notably NGC 128 (Sandage 1961; de Vaucouleurs 1974). This box-shaped bulge shows remarkably large rotation at large z distances. Even at $z = 34''$ (3 h^{-1} kpc), the maximum rotation velocity is still ~ 100 km s^{-1}, comparable to the dispersion in the bulge at that height. In fact, the 27″ perpendicular cut shows that *the velocity is almost constant up to 30″ (3 h^{-1} kpc) above the disk; i.e., the bulge of NGC 4565 is a differentially rotating cylinder up to large distances above the plane.* Only at $z \geq 30''$ does the usual smooth decrease in velocity begin. Cylindrical rotation has also been seen by Davies and Illingworth (1982) in another box-shaped bulge, NGC 1381. We also recall that the particularly box-shaped bulge of NGC 128 rotates very rapidly (Bertola and Capaccioli 1977). This suggests that the structural peculiarity is connected with and perhaps caused by cylindrical rotation. It is interesting to note that several recent n-body models of rapidly rotating systems also show signs of a box-shaped structure (Hohl and Zang 1979; Combes and Sanders 1981). The velocities in the 12″ parallel cut (Fig. 2*c*) arise predominantly from the disk for radii beyond $\sim 30''$. The maximum velocity reached (~ 240–270 km s^{-1}, depending upon the weight given to the last point) agrees quite well with the value 270 km s^{-1} seen in the H I data of Sancisi (1976). The behavior of the dispersion profiles is also unusual in this galaxy. The dispersion remains essentially constant at $\sigma \approx 150$ km s^{-1} out to 15″ from the nucleus and then falls to values $\sigma \lesssim 100$ km s^{-1}.

VI. DISCUSSION

a) Comparison of Bulges and Ellipticals

The primary purpose of this paper is to compare the amount of rotation in bulges and ellipticals. This is done in Figure 3, which is the usual plot of $V_m/\bar{\sigma}$ versus ellipticity ϵ (Illingworth 1977; Binney 1978; see Illingworth 1981 for a review). The factor $V_m/\bar{\sigma}$ is the ratio of the maximum bulge rotation velocity to the mean velocity dispersion, while ϵ is the mean bulge ellipticity in the radius range of the rotation data. Recall that $V_m/\bar{\sigma}$ is a measure of the fraction of the dynamical support of a galaxy which is provided by rotation. That is, $(V_m/\alpha\bar{\sigma})^2$ is the ratio of rotational to random kinetic energy, where $\sqrt{2} \lesssim \alpha \lesssim \sqrt{3}$, depending on the amount of velocity anisotropy. The $V_m/\bar{\sigma} - \epsilon$ diagram has the advantage of using only observed quantities in a distance- and luminosity-independent way. Also, the analogous parameters of projected dynamical models can be defined in a very general way (Binney 1981).

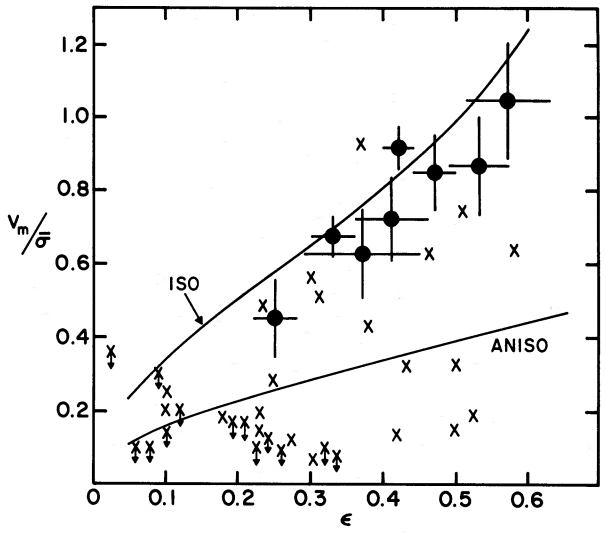

FIG. 3.—Comparison of bulge data (*filled circles*) with all available elliptical galaxy data (*crosses*, *arrows* indicate upper limits) in the dimensionless rotation-ellipticity plane. Derivation of V_m, $\bar{\sigma}$, and ϵ is discussed in the text. The line labeled ISO represents projected models of oblate spheroids with isotropic residual velocities and rotational flattening. The line labeled ANISO describes a typical anisotropic oblate model with σ_z smaller than σ_r and σ_θ.

i) *Derivation of V_m, $\bar{\sigma}$, and ϵ*

Figure 3 illustrates $V_m(0)/\bar{\sigma}$ versus ϵ for all unbarred bulges that have been measured to date (Table 4), including ones that are not edge-on. Data on elliptical galaxies are taken from a summary table in Fried and Illingworth (1982). Since the bulge parameters shown are critical to the interpretation, their derivation will be described in detail.

For galaxies that are not edge-on, V_m can only be derived if the bulge is massive enough so that $V(r)$ reaches a well-defined plateau or maximum at radii dominated by bulge light. This was the case for M31, M81, and NGC 1553. Values of V_m are then read directly from the major-axis rotation curve. However, estimating V_m is not straightforward in edge-on galaxies. These have the advantage that bulges can be measured at lower surface brightness without including disk light. However, bulge velocities are not directly measurable

TABLE 4

ROTATION-ELLIPTICITY RESULTS

Galaxy (1)	V_m (km s^{-1}) (2)	$V_m(0)$ (km s^{-1}) (3)	$\bar{\sigma}$ (km s^{-1}) (4)	$\frac{V_m(0)}{\bar{\sigma}}$ (5)	ε (6)	$\langle V \rangle_{\rm minor}$ (km s^{-1}) (7)
NGC 224	65±15	65±15	145±13	0.45±0.11	0.25±0.03	...
NGC 1553 ...	156±5	156±5	170±10	0.92±0.06	0.42±0.02	...
NGC 3031 ...	100±5	100±5	146±9	0.68±0.05	0.33±0.03	...
NGC 3115 ...	(155±20)	195±20	184±20	1.06±0.16	0.57±0.06	...
NGC 4565 ...	(100±13)	100±13	138±11	0.72±0.11	0.41±0.05	0±3
NGC 4594 ...	(108±19)	130±24	207±14	0.63±0.12	0.37±0.08	8±5
NGC 5866 ...	(118±12)	132±17	152±11	0.87±0.13	0.53±0.04	3±3
NGC 7814 ...	(83±14)	123±12	144±10	0.85±0.10	0.47±0.03	4±6

NOTE.—Sources for data not from this paper. NGC 224: V—Pellet 1976, McElroy 1981; σ—Whitmore 1980, McElroy 1981. NGC 1553: V and σ—Kormendy 1982*a*; ε—Evans 1951. NGC 3031: preliminary data—Illingworth, 1981; Verter *et al.* 1982. NGC 3115: Illingworth and Schechter 1982.

Ellipticity data are derived from photometry sources given in col. (4) of Table 1, supplemented by our own plate material.

Parentheses indicate that V_m is derived from a spectrum offset from the major axis.

along the major axis because of the disk. All of the elliptical galaxy data in Figure 3 were taken along the major axis. We know that V decreases with increasing height z, both from dynamical models and from observations of bulges (this paper) and ellipticals (Davies and Illingworth 1982). Therefore, the V_m values deduced from the offset parallel cuts are too small for direct comparison with E galaxy data. Table 4 accordingly gives two values of V_m for the edge-on galaxies. The first is derived directly from that parallel cut nearest the disk for which we are confident that disk contamination is small. In NGC 4594, 5866, and 7814 V_m is the average of the outermost two or three velocity measurements along the parallel cuts at 30″, 14″, and at 12″ and 18″ (averaged), respectively. Second, we give in Table 4 a value $V_m(0)$ corrected to $z = 0''$ (i.e., the major axis). In NGC 4565 a correction is not necessary because of the cylindrical rotation; we therefore set $V_m(0)$ equal to the mean velocity V_m of the three outermost measurements in the $z = 34''$ spectrum (Fig. 2*e*).

The correction procedure used to determine $V_m(0)$ is an empirical one based on two-dimensional velocity maps of two elliptical galaxies measured by Davies and Illingworth (1982). The elliptical galaxy data define the $V(z)$ gradient at *all* z, whereas our bulge data give $V(z)$ for the bulge only at heights large enough that disk contamination is negligible. We therefore use the functional form of the $V(z)$ relation in ellipticals to extrapolate the $V(z)$ values observed in our bulges to $z = 0$. This requires, first, that all of the $V(z)$ profiles be scaled in z by a photometric length scale. We use as our length scale the "equivalent" radius z_e defined by a de Vaucouleurs (1959) $z^{1/4}$ law fitted to the minor-axis brightness profile (z_e is not a critical parameter). Plots of velocity versus z/z_e and an examination of the photometric data then show that the disk contribution is probably insignificant above $z \approx 0.25 z_e$. Given this result, the elliptical galaxy velocity maps of Davies and Illingworth provide a means of extrapolating $V(z)$ to $z = 0$ in the following way. In both of these ellipticals, and also in a rotationally flattened model from Larson (1975), the extrapolation to $z = 0$ of a straight line fitted by least squares to the $V(z)$ data for $z \geq 0.25 z_e$ is found to be very close to or less than $V(0)$. We therefore use such fits to the bulge data to derive $V_m(0)$. This is a conservative estimate, since the hypothesis being tested is whether bulges rotate more rapidly than ellipticals.

For NGC 4594 and 5866 the above extrapolation of $V(z)$ to $z = 0$ is quoted in Table 4, column (3), as $V_m(0)$. An error estimate is derived by comparing $V_m(0)$ with (*a*) a similar extrapolation to $z = 0$ of the parallel-cut velocities at large radii (which imply larger but very uncertain values of $V_m[0]$), and (*b*) the smaller V_m values in column (2) of Table 4. In NGC 7814, but not in any other galaxy, the $V_m(0)$ values extrapolated from the 20″ and 40″ perpendicular cuts are slightly larger than the actual velocities at $z = 4''$. We have therefore averaged the outermost three points in the 4″ parallel cut to give $V_m(0)$. We have already noted in § V*b* that the contribution in NGC 7814 from any stellar disk is very small above the dust lane.

An appropriate velocity dispersion for evaluating $V_m/\bar{\sigma}$ is obtained as follows. In principle we need a mass-weighted mean $\langle \sigma^2 \rangle$ over the whole bulge, just as the appropriate velocity is a weighted mean $\langle V^2 \rangle$ (Binney 1978, 1980, 1981). These quantities cannot be evaluated without more detailed data and modeling of the unprojected structure. However, Binney (1980) has shown that the ratio V_m/σ_0 of maximum rotation velocity to central velocity dispersion is a good

approximation to $(\langle V^2\rangle/\langle\sigma^2\rangle)^{1/2}$ for isotropic oblate models. It is still difficult to extract an appropriate σ_0 from the measurements, because galaxy nuclei may show dynamical effects not relevant to the structure of the bulge. To ensure that our choice of σ relates to the population measured by V_m, we use a mean dispersion derived from the bulge data *excluding* points at $r \leq 1''.4$. Binney's (1980) models show that a dispersion $\bar{\sigma}$ averaged out to a radius $r \approx 5r_c$, where r_c is the core radius, provides a reasonable approximation to σ_0. Such an average is also much more accurate than a single measurement at $r = 0$. Since in ellipticals $5r_c \approx r_e/2$ (Kormendy 1977), where r_e is the de Vaucouleurs (1959) half-light radius, we average bulge dispersions to $\sim r_e/2$. Data are omitted from regions contaminated by disk light or by dust absorption. Because NGC 4565 is not quite edge-on, data taken within $|z| = 7''$ of the disk are also omitted. The value of the above procedure is that it is well defined and gives results which depend only weakly on the details. The values of $\bar{\sigma}$ in Table 4 are quite well defined. In fact, in many cases the formal error is unrealistically small. To estimate the (more appropriate) external errors, we use the observation of Terlevich *et al.* (1981) that different authors now measure dispersions consistent to $\sim 6\%$. We have therefore added $0.06\bar{\sigma}$ in quadrature to the formal errors to derive the external error estimates given in Table 4.

Ellipticities ε were derived for non–edge-on galaxies from published isophotes referenced in Table 1. However, ε is less easily derived in edge-on galaxies, because the long path length enhances the disk contribution. The values in Table 4 are derived from published photometry, with the disk removed as much as possible. The ellipticities have been averaged in the radius range covered by the velocity data, and are slightly biased toward larger values if ε varies with radius. Only for NGC 4594 is there any serious disagreement between sources; we have adopted an average value.

ii) *The $V_m/\bar{\sigma} - \varepsilon$ Diagram*

The implications of Figure 3 are discussed in terms of dynamical models due to Binney (1978, 1980; see also Illingworth 1977, 1981). The line labeled ISO represents models of oblate-spheroidal systems with isotropic residual velocities. Being isotropic, their flattening is due entirely to rotation. Varying the observed inclination moves such models along the ISO line (Illingworth 1977). As a result, galaxies that are isotropic oblate spheroids will fall on or close to the ISO line irrespective of inclination. The line labeled ANISO is also for an oblate spheroid model, but one in which anisotropy in the velocity distribution contributes to the flattening (Binney 1978).

Figure 3 suggests that bulges rotate more rapidly than elliptical galaxies. They appear to rotate almost as rapidly as oblate-spheroid dynamical models in which all of the flattening is due to rotation. Much of the excess flattening with respect to the ISO line in Figure 3 may be due to the disk potential (see Monet, Richstone, and Schechter 1981); however, the magnitude of this effect is difficult to evaluate. Possibly the adopted V_m is also too small for some edge-on galaxies if the data do not reach large enough radii. Thus, the bulge data are more consistent with isotropic residual motions than Figure 3 would suggest. *The amount of anisotropy implied by the observations is small*, especially because the $V_m/\bar{\sigma}$ value required for a particular flattening decreases rapidly as the axial dispersion is decreased below the dispersion in the equatorial plane (see Fig. 1*a* of Binney 1981). Neglecting the effect of the disk potential, the distribution of bulge points in Figure 3 is formally consistent with a ratio of axial-to-radial dispersion $\sigma_z/\sigma_r \approx 0.97$ (using Binney 1981). *The data are consistent with the assumption that bulges are oblate spheroids.*

These results imply that bulges are much more uniform in their rotation properties than ellipticals. This is demonstrated further in Figure 4. Figure 4 shows the distribution of $(V/\sigma)^* = (V_m/\bar{\sigma})_{\rm observed}/(V/\sigma)_{\rm ISO}$ for the bulges and ellipticals in Figure 3. While ellipticals typically rotate slowly (and so are anisotropy dominated), 10%–15% of them rotate rapidly enough to be consistent with oblate spheroid models. The bulges show much less dispersion. It is unlikely that this result is due to the small size of our galaxy sample. Figures 3 and 4 contain galaxies with a range of types from S0 to Sb, and with a range of bulge-to-disk ratios from 11/1 to 1/4. Since we are studying the largest, least flattened bulges, i.e., those which are most like elliptical galaxies, it is likely that rotation generally dominates the dynamics of bulges. Partial confirmation is provided by Kormendy's (1982*b*) conclusion that the bulges of barred galaxies rotate even more rapidly than the present bulges.

The above discussion is subject to an important caveat. Schechter (1981) has emphasized the fact that NGC 4594 contains the only bulge in our sample that is as bright as the average elliptical in Figure 3. This point is illustrated in Figure 5. The bulge magnitudes of M31, NGC 3115, 4594, and 5866 are well established by published photometry. No plausible errors in bulge-to-disk ratio can seriously affect the conclusion that our bulges are ~ 2 mag fainter than the average elliptical in Figure 3. While the numbers are small, those ellipticals which, like most of our bulges, are fainter than $M_B = -21$, are found to rotate marginally faster than brighter ellipticals (Fried and Illingworth 1982). However, M32 is currently that only elliptical studied that is very faint. It essentially satisfies the $V_m/\bar{\sigma} - \varepsilon$ line condition for isotropic spheroids. The other ellipticals fainter than $M_B = -21$ still rotate much less than typical bulges. Thus, the available data offer no compelling reason to believe that the kinematic difference which we see between bulges and ellipticals is purely a luminosity effect.

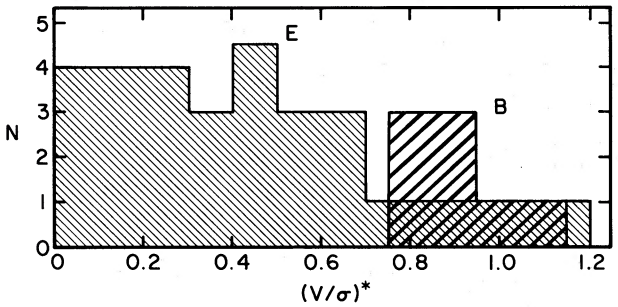

FIG. 4.—The relative frequency (i.e., number N) of ellipticals (E) and bulges (B) with different values of $(V/\sigma)^* = (V/\sigma)_{\text{observed}}/(V/\sigma)_{\text{isotropic models}}$.

Nevertheless, *we conclude only that bulges which typically have* $-18.5 \geq M_B \geq -21$ *rotate more rapidly than ellipticals with* $-19.5 \geq M_B \geq -23.5$. Rotation measurements of faint ellipticals are urgently needed to explore the dependence of $(V/\sigma)^*$ on luminosity. A recently completed study by Davies *et al.* (1982) shows that much of the kinematic difference that we see between bulges and ellipticals is, in fact, due to the luminosity difference. On the other hand, the bulge of NGC 4594 ($M_B = -22.2$) rotates as rapidly as the fainter bulges and much more rapidly than the average elliptical of comparable brightness. Clearly, we also need to investigate more such bright bulges.

In general, most elliptical galaxies studied to date are slowly rotating systems whose flattening is due to anisotropy, whereas bulges are rotationally flattened oblate spheroids. However, it is important to note that their respective distributions of points overlap in the $V_m/\bar{\sigma} - \varepsilon$ diagram. It is an exaggeration to suggest (Bertola and Capaccioli 1978) that there is a dichotomy in the dynamical properties of bulges and ellipticals. There is also a continuum in photometric properties. Several galaxies studied here contain $\lesssim 10\%$ contribution from a disk. There almost certainly exist galaxies which are still closer to being ellipticals in the sense that their disks contribute an even smaller fraction of the light (Kormendy 1979, 1980). There appears to be no dichotomy in the structure of elliptical and disk galaxies.

b) Dynamical Properties of Bulges

The present observations and those of NGC 3115 by Illingworth and Schechter (1982) constitute the most detailed kinematic mapping available for any stellar system. Clearly, we can learn more from the data than is contained in the global parameters discussed in the previous section. Fully exploiting the data requires the construction of dynamical models which are beyond the scope of this paper. However, several points are briefly worth mentioning.

For example, we have already indicated that there are significant variations in the form of the two-dimensional velocity field. Three of our bulges behave like early collapse models (e.g., Larson 1975) in which differentially rotating spheroids were formed that had rotation velocities decreasing with increasing height z. However, the box-shaped bulge of NGC 4565 is in *cylindrical* rotation. That is, $V(z)$ is essentially constant with z to heights of several kpc above the disk. The implication is that the boxlike structure is dynamically related to rapid cylindrical rotation (see also Davies and Illingworth 1982; Illingworth and Kormendy 1982). In particular, since V does not decrease rapidly with increasing z, the fraction of the total kinetic energy which is in rotation is larger than in the other bulges, despite the fact that all have similar $(V/\sigma)^*$ values. In fact, in an isotropic E4 system the fraction of the dynamical support which is in rotation is a factor of $\sim(1.16/0.99)^2 = 1.37$ larger when the rotation is cylindrical than when it is spheroidal (Table 1 of Binney 1980). This is a dynamically significant difference, which may indicate that both rapid

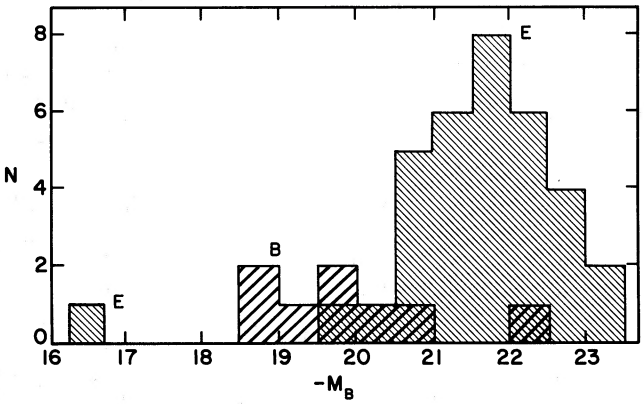

FIG. 5.—The relative frequency of ellipticals (E) and bulges (B) in Figs. 3 and 4 which have absolute magnitude M_B. The magnitude zero point is based on $H_0 = 50$ km s^{-1} Mpc^{-1}.

rotation and rotation on cylinders is required to produce a box-shaped bulge.

Another property of our galaxies which is apparent in Figure 2 and Table 4 (col. [7]) is the fact that the rotation velocities $\langle V \rangle_{\rm minor}$ along the minor axes are consistent with zero to high accuracy. $\langle V \rangle_{\rm minor}$ is a weighted mean rotation velocity; the weights are proportional to $\epsilon(V)^{-2}$, and the $r = 0$ point has been omitted from the average. It is well known that triaxial ellipsoids can show rotation about their minor axes if viewed at skew orientations from outside their kinematic equational plane (Williams 1981). In our edge-on disk galaxies we expect that the bulges are also seen edge-on. That is, it is very unlikely that the disk and bulge would have different rotation axes because the restoring torques would be very large. The photometric minor axis is then also the rotation axis and should therefore show no rotation even if the bulge is triaxial. Thus, the apparent lack of minor-axis rotation in the present bulges is not an argument against triaxiality. Any triaxiality is, however, small because the observed $V_m/\bar{\sigma}$ values in Figure 3 are essentially consistent with the oblate-spheroid models.

c) *Implications for Theories of Galaxy Formation*

The present data provide considerable support for classical collapse models of disk galaxy formation. Virtually all of the bulges studied to date fall in the region of the $V_m/\bar{\sigma} - \epsilon$ diagram defined by these models, both dissipational (Larson 1975, 1976) and dissipationless (Gott 1975; see Illingworth 1977 for the positions of the models). Indeed, the uniformity in the dynamical properties of bulges is striking (see Figs. 3 and 4 and contrast the diversity of E galaxy properties). Given then that the conventional approach to galaxy formation is a reasonable approximation for disk galaxies, we can now clarify the picture somewhat with regard to the role played by dissipation.

The importance of dissipation in bulge formation is already indicated by the observed color gradients (Faber 1977) and high central densities. In addition, the existence of a disk implies that much of the material that formed the visible part of a galaxy was highly dissipative. Further evidence for the importance of dissipation now comes from the large amount of rotation seen in bulges. We can compare the observed rotation with that expected to be acquired through tidal torques by using the dimensionless rotation parameter λ (Peebles 1971; Fall 1980)

$$\lambda = J|E|^{1/2}G^{-1}M^{-5/2}. \quad (1)$$

Here J, E, and M are the total angular momentum, energy, and mass, respectively, and G is the gravitational constant. The usefulness of λ stems from the ease with which it can be derived for numerical and theoretical models. In general, $\lambda \propto V/\sigma$. Now, theoretical calculations (Peebles 1969) and N-body models (Peebles 1971; Efstathiou and Jones 1979) of the galaxy-formation era both suggest that the amount of rotation produced by tidal torques is small, $\langle \lambda \rangle \approx 0.06$. This is comparable to the amount of rotation observed in bright ellipticals. Increasing $\langle \lambda \rangle$ to ~ 0.3, as seen in the present bulges, essentially requires dissipation during the formation process.

The detailed velocity fields are also consistent with dissipational formation theories. Early models of this kind include Larson's (1975, 1976) studies of the nonhomologous collapse of a gaseous protogalaxy with simultaneous star formation. The velocity and velocity dispersion fields of Larson's models are in qualitative agreement with our data. For example, both show smoothly decreasing rotation velocities with increasing height z. Also both have rotation curves which become more linear as z increases.

If the dissipative collapse picture is appropriate for the formation of disk galaxies, can an appropriate variation of this approach produce realistic ellipticals? Certainly the faint ellipticals studied by Davies *et al.* (1982) are kinematically similar enough to bulges to plausibly be formed by a dissipational collapse process. Much brighter elliptical galaxies also have high central densities and color gradients suggestive of dissipational formation. However, the low rotation rates in bright ellipticals and the attendant anisotropy required to account for their flattening complicate the picture considerably. The difficulty is that dissipation must have been weak enough to preserve the low rotation rates and anisotropic residual motions, but effective enough to produce color gradients and high central densities. The large range in dynamical properties of bright ellipticals, as compared with the uniformity of bulges, must also be explained. Finally, no material can remain to form a disk. As noted in § VI*b*, this may turn out to be a crucial observation. In terms of photometric properties and stellar content, the bulges of NGC 3115, 4594, 5866, and 7814 are very like ellipticals. They contribute fully 80%–90% of the light in these galaxies, and all four rotate rapidly. No galaxies of similar bulge-to-disk ratio are known whose bulges rotate as slowly as bright ellipticals. Even the very luminous bulge of NGC 4594 rotates rapidly. Can formation theories be constructed which have enough dissipation to produce realistic ellipticals without having any even more dissipative material left over to make a disk, or is another, different mechanism required to prevent disk formation in ellipticals?

A detailed investigation of the possible formation of ellipticals by a variation of the dissipational collapse picture would therefore be very valuable. If it becomes impossible to reconcile the dynamical and photometric data with such models, then an additional formation

mechanism may be required. One popular possibility is that some ellipticals originated through mergers of disk galaxies (Toomre 1977; Jones and Efstathiou 1979; Fall 1980). Problems with this picture are discussed by Ostriker (1980); a more viable approach may be to assume that the mergers occur while the material is still gaseous (Searle 1977; Fall 1980; Norman and Silk 1981). An attractive feature of the merger process is the tendency to produce ellipticals with a large diversity in dynamical properties. It seems likely, both on observational and theoretical grounds, that *some* ellipticals are merger remnants. We now need to know whether or not the observed kinematics require that *most* ellipticals formed through mergers.

VII. SUMMARY

1. Bulges with $-M_B \approx 18.5$–21 generally rotate more rapidly than elliptical galaxies with $-M_B \approx 19.5$–23.5. Most bulges closely satisfy the $V_m/\bar{\sigma} - \varepsilon$ relationship for oblate-spheroid dynamical models that owe their flattening to rotation. Small deviations of the bulge data below this relationship may be due to excess flattening produced by the disk potential. In contrast to ellipticals, in which the residual velocity distribution is generally anisotropic, the present data are consistent with the assumption that bulges are spheroids with nearly isotropic residual velocities.

2. The two-dimensional velocity fields have the following properties. Rotation velocities decrease smoothly with increasing distance from the equatorial plane, with no sharp distinction between bulge and disk. Rotation curves measured parallel to the disk, but displaced from it, rise more slowly and more linearly than major-axis velocities. The velocity dispersions drop away from the nucleus, but then change only slowly, if at all, throughout the bulge.

3. The box-shaped bulge of NGC 4565 has a particularly large amount of rotational energy. This is due to the fact that velocity is constant on cylinders up to large distances from the disk. These and similar observations of NGC 128 (Bertola and Capaccioli 1977) and NGC 1381 (Davies and Illingworth 1982) suggest that the box-shaped structure of such bulges is connected with cylindrical rotation.

4. There may be a physical connection between the kinematic differences found here between bulges and ellipticals and photometric differences found by Kormendy (1980) and by Boroson and Kormendy (1982). In agreement with the above authors we find indications that bulges are generally flatter than the $\sim$ E4 shape characteristic of elliptical galaxies.

5. The distributions of rotation properties of bulges and ellipticals are overlapping. There is no dichotomy in the properties of ellipticals and disk galaxies, as has been suggested by Bertola and Capaccioli (1978).

6. The kinematic properties of bulges are strikingly uniform, in contrast to ellipticals. Together with photometric data, the large amount of rotation suggests that bulge formation was a dissipational process. The global rotation rate and detailed velocity fields are consistent with dissipational collapse theories of galaxy formation.

7. The formation of elliptical galaxies is complicated by the diversity of their properties. We now need to know whether an appropriate variation of the classical collapse picture can reproduce observations indicative of dissipation without resulting in too much rotation and without producing a disk. If this proves to be difficult, a more complicated way of forming elliptical galaxies, such as mergers of disk galaxies, may be required.

We are most grateful to P. Schechter for making available his Fourier quotient program for the present work and to J. Fried and D. McElroy for extensive development and maintenance work on the program. We thank W. Ditsler and J. De Veny for their efficient engineering support of the HGVS, and B. Schueler for her patience and competence with the manuscript. Finally, we gratefully acknowledge helpful conversations with or comments on the manuscript from J. Binney, T. Boroson, A. Bosma, R. Davies, G. Efstathiou, M. Fall, I. King, C. Norman, P. Schechter, and F. Schweizer.

REFERENCES

Babcock, H. W. 1939, *Lick Obs. Bull.* **19**, 41.
Bertola, F., and Capaccioli, M. 1975, *Ap. J.*, **200**, 439
_____. 1977, *Ap. J.*, **211**, 697.
_____. 1978, *Ap. J.* (*Letters*), **219**, L95.
Binney, J. 1976, *M.N.R.A.S.*, **177**, 19.
_____. 1978, *M.N.R.A.S.*, **183**, 501.
_____. 1980, *M.N.R.A.S.*, **190**, 421.
_____. 1981, in *Structure and Evolution of Normal Galaxies*, ed. S. M. Fall and D. Lynden-Bell (Cambridge: Cambridge University Press), p. 55.
Blaauw, A. 1965, in *Stars and Stellar Systems*, Vol. **5**, *Galactic Structure*, ed. A. Blaauw and M. Schmidt (Chicago: University of Chicago Press), p. 435.
Boroson, T., and Kormendy, J. 1982, in preparation.
Bottinelli, L., Gouguenheim, L., and Paturel, G. 1980, *Astr. Ap. Suppl.*, **40**, 355.
Burkhead, M. S. 1979, in *Photometry, Kinematics and Dynamics of Galaxies*, ed. D. S. Evans (Austin: Department of Astronomy, University of Texas at Austin), p. 143.
Burstein, D., and Heiles, C. 1978, *Ap. J.*, **225**, 40.
Combes, F., and Sanders, R. H. 1981, *Astr. Ap.*, **96**, 164.
Davies, R. L. 1981, *M.N.R.A.S.*, **194**, 879.
Davies, R. L., Efstathiou, G., Fall, S. M., Illingworth, G., and Schechter, P. L. 1982, in preparation.
Davies, R. L., and Illingworth, G. 1982, in preparation.
de Vaucouleurs, G. 1958, *Ap. J.*, **128**, 465.
_____. 1959, *Handbuch der Physik*, **53**, 311.
_____. 1974, in *IAU Symposium 58, The Formation and Dynamics of Galaxies*, ed. J. R. Shakeshaft (Dordrecht: Reidel), p. 335.
_____. 1975 , in *Stars and Stellar Systems*, Vol. **9**, *Galaxies and the Universe*, ed. A. Sandage, M. Sandage, and J. Kristian (Chicago: University of Chicago Press), p. 557.

de Vaucouleurs, G. 1978, *Ap. J.*, **223**, 730.
de Vaucouleurs, G., de Vaucouleurs, A., and Corwin, H. G. 1976, *Second Reference Catalogue of Bright Galaxies* (Austin: University of Texas Press).
Efstathiou, G., Ellis, R. S., and Carter, D. 1980, *M.N.R.A.S.*, **193**, 931.
Efstathiou, G., and Jones, B. J. T., 1979, *M.N.R.A.S.*, **186**, 133.
Evans, D. S. 1951, *M.N.R.A.S.*, **111**, 526.
Faber, S. M. 1977, in *The Evolution of Galaxies and Stellar Populations*, ed. B. M. Tinsley and R. B. Larson (New Haven: Yale University Observatory), p. 157.
Faber, S. M., Balick, B., Gallagher, J. S., and Knapp, G. R. 1977, *Ap. J.*, **214**, 383.
Faber, S. M., and Jackson, R. E. 1976, *Ap. J.*, **204**, 668.
Fall, S. M. 1980, *Ann. NY Acad. Sci.*, **336**, 172.
Ford, W. K., Jr. 1979, *Ann. Rev. Astr. Ap.*, **17**, 189.
Freeman, K. C. 1975, *Stars and Stellar Systems*, Vol. **9**, *Galaxies and the Universe*, ed. A. Sandage, M. Sandage, and J. Kristian (Chicago: University of Chicago Press), p. 409.
Fried, J., and Illingworth, G. 1982, in preparation.
Gott, J. R., III. 1975, *Ap. J.*, **201**, 296.
Hamabe, M., Kodaira, K., Okamura, S., and Takase, B. 1979*a*, *Pub. Astr. Soc. Japan*, **31**, 431.
_____. 1979*b*, in *Photometry, Kinematics and Dynamics of Galaxies*, ed. D. S. Evans (Austin: Department of Astronomy, University of Texas at Austin), p. 109.
_____. 1980, private communication.
Hohl, F., and Zang, T. A. 1979, *A.J.*, **84**, 585.
Illingworth, G. 1977, *Ap. J. (Letters)*, **218**, L43.
_____. 1981, in *Structure and Evolution of Normal Galaxies*, ed. S. M. Fall and D. Lynden-Bell (Cambridge: Cambridge University Press), p. 27.
Illingworth, G., and Kormendy, J. 1982, in preparation.
Illingworth, G., and Schechter, P. L. 1982, *Ap. J.*, **256**, 481.
Jones, B. J. T., and Efstathiou, G. 1979, *M.N.R.A.S.*, **189**, 27.
Kormendy, J. 1977, *Ap. J.*, **218**, 333.
_____. 1979, in *Photometry, Kinematics and Dynamics of Galaxies*, ed. D. S. Evans (Austin: Department of Astronomy, University of Texas at Austin), p. 341.
_____. 1980, in *ESO Workshop on Two Dimensional Photometry*, ed. P. Crane and K. Kjär (Geneva: ESO), p. 191.
_____. 1982*a*, in preparation.
_____. 1982*b*, *Ap. J.*, **257**, in press.
Kormendy, J., and Illingworth, G. 1982, in preparation.
Larson, R. B. 1975, *M.N.R.A.S.*, **173**, 671.
_____. 1976, *M.N.R.A.S.*, **176**, 31.
McElroy, D. 1981, Ph.D. thesis, Arizona State University.
Monet, D. G., Richstone, D. O., and Schechter, P. L. 1981, *Ap. J.*, **245**, 454.
Norman, C. A., and Silk, J. 1981, *Ap. J.*, **247**, 59.
Oort, J. H. 1965, in *Stars and Stellar Systems*, Vol. **5**, *Galactic Structure*, ed. A. Blaauw and M. Schmidt (Chicago: University of Chicago Press), p. 455.
Ostriker, J. P. 1980, *Comments Ap.*, **8**, 177.
Peebles, P. J. E. 1969, *Ap. J.*, **155**, 393.
_____. 1971, *Astr. Ap.*, **11**, 377.
Pellet, A. 1976, *Astr. Ap.*, **50**, 421.
Peterson, C. J. 1978*a*, *Ap. J.*, **221**, 80.
_____. 1978*b*, *Ap. J.*, **222**, 84.
Prendergast, K. H., and Tomer, E. 1970, *A.J.*, **75**, 674.
Richstone, D. O., and Schectman, S. A. 1980, *Ap. J.*, **235**, 30.
Rubin, V. C., Ford, W. K., Jr., and Kumar, C. K. 1973, *Ap. J.*, **181**, 61.
Sancisi, R. 1976, *Astr. Ap.*, **53**, 159.
Sandage, A. 1961, *Hubble Atlas of Galaxies* (Washington: Carnegie Institution of Washington).
Sandage, A., Freeman, K. C., and Stokes, N. R. 1970, *Ap. J.*, **160**, 831.
Sandage, A., and Tammann, G. A. 1976, *Ap. J.*, **210**, 7.
Sargent, W. L. W., Schechter, P. L., Boksenberg, A., and Shortridge, K. 1977, *Ap. J.*, **212**, 326 (S^2BS).
Schechter, P. L. 1980, *A.J.*, **85**, 801.
_____. 1981, private communication.
Schechter, P. L., and Gunn, J. E. 1979, *Ap. J.*, **229**, 472 (SG).
Schweizer, F. 1978, *Ap. J.*, **220**, 98.
_____. 1981, private communication.
Searle, L. 1977, in *The Evolution of Galaxies and Stellar Populations*, ed. B. M. Tinsley and R. B. Larson (New Haven: Yale University Observatory), p. 219.
Tammann, G. A., and Sandage, A. 1968, *Ap. J.*, **151**, 825.
Terlevich, R., Davies, R. L., Faber, S. M., and Burstein, D. 1981, *M.N.R.A.S.*, **196**, 381.
Tonry, J., and Davis, M. 1979, *A.J.*, **84**, 1511.
Toomre, A. 1977, in *The Evolution of Galaxies and Stellar Populations*, ed. B. M. Tinsley and R. B. Larson (New Haven: Yale University Observatory), p. 401.
Tsikoudi, V. 1977, *Pub. Astr. Univ. Texas*, No. 10.
van Houten, C. J. 1961, *Bull. Astr. Inst. Netherlands*, **16**, 1.
Verter, F., Binney, J., Illingworth, G., and McElroy, D. 1982, in preparation.
Westphal, J. A. 1972, *Carnegie Yrb.*, **71**, 705.
Whitmore, B. C. 1980, *Ap. J.*, **242**, 53.
Whitmore, B. C., and Kirshner, R. P. 1981, *Ap. J.*, **250**, 43.
Whitmore, B. C., Kirshner, R. P., and Schechter, P. L. 1979, *Ap. J.*, **234**, 68.
Williams, T. B. 1977, *Ap. J.*, **214**, 685.
_____. 1981, *Ap. J.*, **244**, 458.
Wilson, C. P. 1975, *A.J.*, **80**, 175.
Young, P., Sargent, W. L. W., Boksenberg, A., Lynds, C. R., and Hartwick, F. D. A. 1978, *Ap. J.*, **222**, 450.

GARTH ILLINGWORTH: Kitt Peak National Observatory, P.O. Box 26732, Tucson, AZ 85726

JOHN KORMENDY: Dominion Astrophysical Observatory, 5071 W. Saanich Rd., Victoria, BC V8X 4M6 Canada

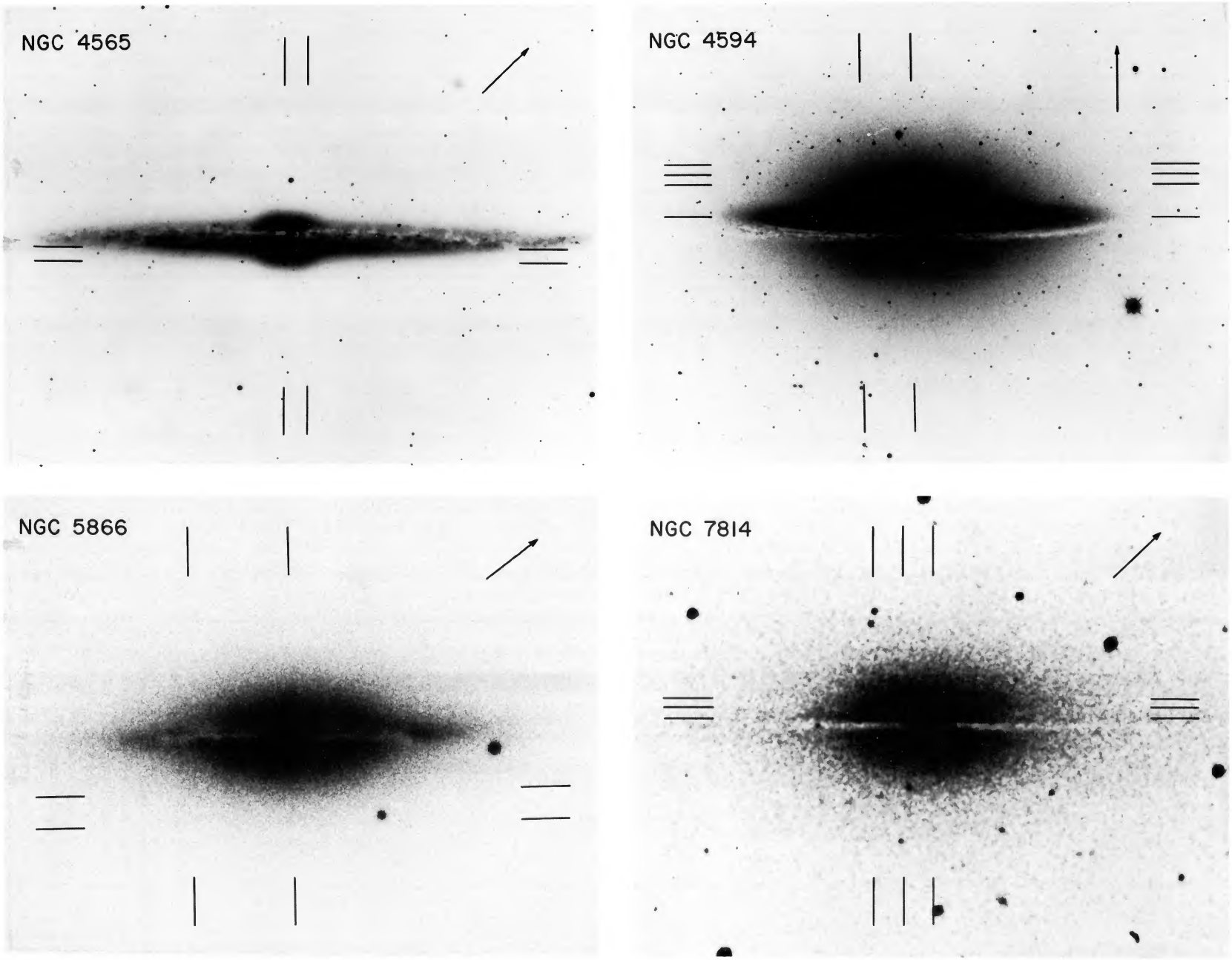

FIG. 1.—The four S0–Sb galaxies studied. Arrow indicates north in each case. East is counterclockwise in the usual sense. The length of the arrow is 95″, 62″, 16″, and 43″, respectively, in NGC 4565, 4594, 5866, and 7814. Horizontal and vertical bars show the slit positions for the offset spectra (see Fig. 2 and Table 3 for the actual offsets).